Mon. Not. R. Astron. Soc. **000**, 1–?? (2013) Printed 14 July 2016 (MN LATEX style file v2.2)

Fundamental properties of $Kepler$ and $CoRoT$ targets: III. Tuning scaling relations using the first adiabatic exponent

M. Yıldız⋆, Z. Çelik Orhan and C. Kayhan

Department of Astronomy and Space Sciences, Science Faculty, Ege University, 35100, Bornova, İzmir, Turkey

arXiv:1607.03768v1 [astro-ph.SR] 13 Jul 2016

Accepted 2013 May 15. Received 2013 April 11; in original form 2013 April 11

ABSTRACT

So called scaling relations have the potential to reveal the mass and radius of solar-like oscillating stars, based on oscillation frequencies. In derivation of these relations, it is assumed that the first adiabatic exponent at the surface (Γ_{1s}) of such stars is constant. However, by constructing interior models for the mass range 0.8-1.6 $M_{\odot}$, we show that Γ_{1s} is not constant at stellar surfaces for the effective temperature range with which we deal. Furthermore, the well-known relation between large separation and mean density also depends on Γ_{1s}. Such knowledge is the basis for our aim of modifying scaling relations. There are significant differences between masses and radii found from modified and conventional scaling relations. However, comparison of predictions of these relations with the non-asteroseismic observations of Procyon A reveals that new scaling relations are effective in determining the mass and radius of stars. In the present study, solar-like oscillation frequencies of 89 target stars (mostly *Kepler* and *CoRoT*) were analysed. As well as two new reference frequencies ($\nu_{\rm min1}$ and $\nu_{\rm min2}$) found in the spacing of solar-like oscillation frequencies of stellar interior models, we also take into account $\nu_{\rm min0}$. In addition to the frequency of maximum amplitude, these frequencies have very strong diagnostic potential for determination of fundamental properties. The present study involves the application of derived relations from the models to the solar-like oscillating stars, and computes their effective temperatures using purely asteroseismic methods. There are in general very close agreements between effective temperatures from asteroseismic and non-asteroseismic (spectral and photometric) methods. For the Sun and Procyon A, for example, the agreement is almost total.

Key words: stars: evolution – stars: interiors – stars: late-type – stars: oscillations – stars: fundamental parameters

1 INTRODUCTION

Many different types of physical processes occur deep inside stars. The standard stellar models (SSMs), however, are constructed by taking into account only the most basic of the most essential physical principles (such as structure equations, matter-matter and matter-radiation interactions). Therefore, it is inevitable that our SSMs will be inadequate in some respects. Progress depends on finding discrepancies between SSMs and stars. Very detailed analysis is required for improvement in stellar physics, and also for discovering new processes occuring inside stars, and only very precise constraints can lead to the discovery of such processes. Helioseismology and asteroseismology of solar-like oscillating stars are able to provide such constraints (see e.g. Kosovichev 2011, Chaplin & Miglio 2013, Christensen-Dalsgaard 2002, 2016).

Oscillation frequencies (ν) of such stars are now available from the $Kepler$ (Borucki et al. 2010) and $CoRoT$ (Baglin et al. 2006) space missions, and from ground-based observations (Bedding et al. 2010, Bedding et al. 2007 and Bazot et al. 2012). According to scaling relations, stellar mass (M) and radius (R) can be found from frequency of maximum amplitude ($\nu_{\rm max}$), the large separation between the oscillation frequencies ($\Delta\nu$) and effective temperature ($T_{\rm eff}$). $\Delta\nu$ is not constant and therefore its mean value ($\langle\Delta\nu\rangle$) is used in these computations. Furthermore, it has an oscillatory component. We have shown in two recent papers (Yıldız et al. 2014, hereafter Paper I; Yıldız , Çelik Orhan & Kayhan 2015, hereafter Paper II) that there is very strong diagnostic potential in the new reference frequencies ($\nu_{\rm min1}$ and $\nu_{\rm min2}$) at which $\Delta\nu$ is minimum.

Paper I involved the investigations of models constructed using the ANKİ code for the solar-like oscillating stars with solar composition, revealing for the first time new relations between oscillation frequencies and fundamental stellar parameters. The discovery of new reference frequencies $\nu_{\rm min1}$ and $\nu_{\rm min2}$ made these

⋆ E-mail: mutlu.yildiz@ege.edu.tr

relations available. In order to derive general relations, the effects of metallicity (Z) and helium abundance (Y) should be clarified. In Paper II, we attempted to generalize the relations for arbitrary M, R, Z and Y values. In the present study, we analyse observed oscillation frequencies, confirm the relations between the reference frequencies, and apply the new methods to the $Kepler$ and $CoRoT$ target stars. Their $T_{\rm eff}$, R and M were found using asteroseismic parameters. Such an application is also very important for testing the scaling relations.

In derivation of the scaling relations used to compute M and R in terms of $\nu_{\rm max}$, $\langle\Delta\nu\rangle$ and $T_{\rm eff}$, it is assumed that the first adiabatic exponent ($\Gamma_{1\rm s}$) and mean molecular weight (μ) at stellar surface are constant (Brown et al. 1991; Kjeldsen & Bedding 1995). We test whether these quantities are constant for our purposes and, if not, recommend that the scaling relations should be verified (see Section 3).

The relation between $\langle\Delta\nu\rangle$ and mean density ($\langle\rho\rangle$) has been widely discussed in recent papers. White et al. (2011) state that the $\langle\Delta\nu\rangle$-$\langle\rho\rangle$ relation depends on $T_{\rm eff}$ and suggest a fitting formula for correction in order to find $\langle\rho\rangle$ from the observed values of $\langle\Delta\nu\rangle$. In addition to the $\langle\Delta\nu\rangle$-$\langle\rho\rangle$ relation, Belkacem et al. (2013) also discuss the relation between $\nu_{\rm max}$ and acoustic cut-off frequency ($\nu_{\rm ac}$), claiming that departure from the observed relation arises from the complexity of non-adiabatic processes. García Hernández et al. (2015), however, derive an observational scaling ($\langle\Delta\nu\rangle$-$\langle\rho\rangle$) relation for the δ Scuti components in eclipsing binaries. Recently, Sharma et al. (2016) aimed to generalize problems pertaining to the scaling relations for *Kepler* red giants, without considering $\Gamma_{1\rm s}$ as variable. Our strategy is first to identify whether $constants$ are constant, before attempting to find parameters for $\langle\Delta\nu\rangle$-$\langle\rho\rangle$ and $\nu_{\rm max}$-$\nu_{\rm ac}$ relations.

For the assessment of the results on fundamental properties of stars, it is crucial to derive the observed values of these parameters by alternative direct methods, for which, the roles of Sun and Procyon A are of key importance. From astrometric observations of Procyon by $Hubble\ Space\ Telescope$, the mass of its primary component is determined very precisely, 1.478 ± 0.012 M$_\odot$ (Bond et al. 2015). This data enables the testing of new scaling relations (see Section 4). In addition to interferometrically observed solar-like oscillating stars (Huber et al. 2011b, Baines et al. 2014), component stars in eclipsing binaries are benchmark for asteroseismic studies (Gaulme et al. 2013, Rawls et al. 2016), despite the complicating factor of tidally induced oscillations.

This paper is organized as follows. Section 2 is the presentation of the basic asteroseismic and non-asteroseismic properties of the target stars compiled from literature. In this section, we also compare $\nu_{\rm min1}$ and $\nu_{\rm min2}$ of the models with their observational counterparts. Section 3 is devoted to MESA (Paxton et al. 2011) models and role of $\Gamma_{1\rm s}$ in new scaling relations. In this section, we also develop new expressions for effective temperature by using oscillation frequencies. In Section 4, the results based on asteroseismic methods are presented and compared with results obtained by conventional methods. Finally, in Section 5, conclusions are drawn.

2 ASTEROSEISMIC AND NON-ASTEROSEISMIC PROPERTIES OF *Kepler* AND *CoRoT* SOLAR-LIKE OSCILLATING STARS

The basic data of certain *Kepler* (79 stars) and *CoRoT* (7 stars) target stars, compiled from the literature, are listed in Table A1. Oscillation frequencies of three stars (Procyon A, HD 2151 and HD 146233) were obtained from ground-based observations (Bedding et al. 2010, Bedding et al. 2007 and Bazot et al. 2012, respectively). These stars are also listed in this table, with data for the Sun for comparison. For most stars, we provide $B-V$ and $V-K$ colours (SIMBAD database) from photometric, and surface gravity ($\log(g)$), effective temperature ($T_{\rm eS}$) and metallicity ([Fe/H]) from spectroscopic observations.

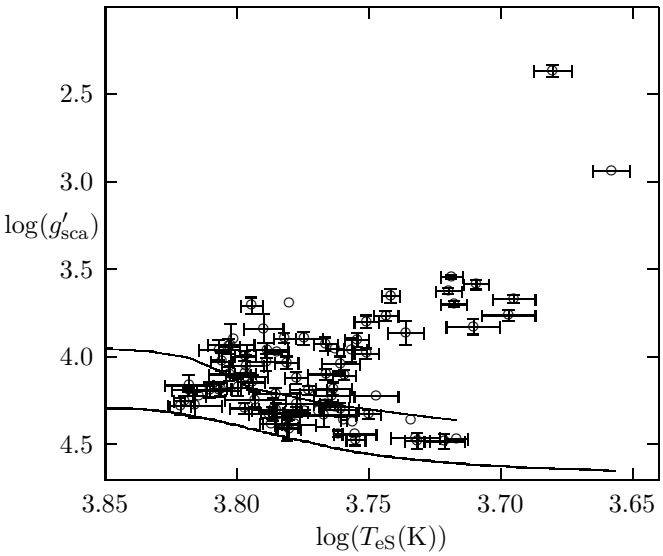

Figure 1. $\log(g'_{\rm sca})$ of the target stars, computed from $\nu_{\rm max}T_{\rm eS}^{0.5}$, is plotted with respect to $\log(T_{\rm eS})$. The thin and thick solid lines represent ZAMS and TAMS lines taken from Yıldız (2015), respectively.

Observational oscillation frequencies are obtained from the *Kepler* and *CoRoT* light curves, and from the radial velocity curves. For most stars, frequencies (ν_{nl}) of modes with low degrees (l) and high order (n) are available, allowing the computation of $\nu_{\rm max}$, $\Delta\nu$ and small separation between oscillation frequencies ($\delta\nu_{02}=\nu_{n0}-\nu_{n-1,2}$). Mean values of $\Delta\nu$ ($\langle\Delta\nu\rangle$) and $\delta\nu_{02}$ ($\langle\delta\nu_{02}\rangle$) are used in scaling relations. Furthermore, two minima are seen in the $\Delta\nu$-ν graph of the majority of stars. For a few stars, there are more than two minima, allowing the consideration of the effect of He II ionization zone on the oscillation frequencies, and the assessment of their diagnostic potential if any. High frequency minima (minH) and low frequency minima (minL) are refered to as $\nu_{\rm minH}$ and $\nu_{\rm minL}$, respectively.

These stars are plotted on a $\log(g'_{\rm sca})$-$\log(T_{\rm eS})$ diagram in Fig. 1. $g'_{\rm sca}$ is computed from conventional scaling relation ($g'_{\rm sca}/g_\odot=\nu_{\rm max}/\nu_{{\rm max}\odot}(T_{\rm eS}/T_{{\rm eff}\odot})^{0.5}$). Uncertainties in $g'_{\rm sca}$ are computed from uncertainties in $\nu_{\rm max}$ and $T_{\rm eS}$ in the standard way: $\Delta g'_{\rm sca}/g'_{\rm sca}=\Delta\nu_{\rm max}/\nu_{\rm max}+0.5\Delta T_{\rm eS}/T_{\rm eS}$. Also seen in Fig. 1 are zero-age main-sequence (ZAMS) and terminal-age main-sequence (TAMS) lines taken from Yıldız (2015). Nearly half are main-sequence (MS) stars while the other half are evolved as far as the red giant phase. $T_{\rm eS}$ of the hottest and coolest stars are about 6630 K (KIC 11081729) and 4550 K (KIC 8219268), respectively. $T_{\rm eS}$ of the coolest MS star (KIC 11772920) is 5209 K. Therefore, the effective temperature range for the models that are used to derive relations between asteroseismic and non-asteroseismic quantities is set as 5200-6650 K (see Section 3).

The colours $B-V$ and $V-K$ derived from atmospheric models (Lejeune, Cuisinier & Buser 1998) were fitted to the observed colours, in order to find the effective temperatures $T_{\rm eBV}$ and $T_{\rm eVK}$,

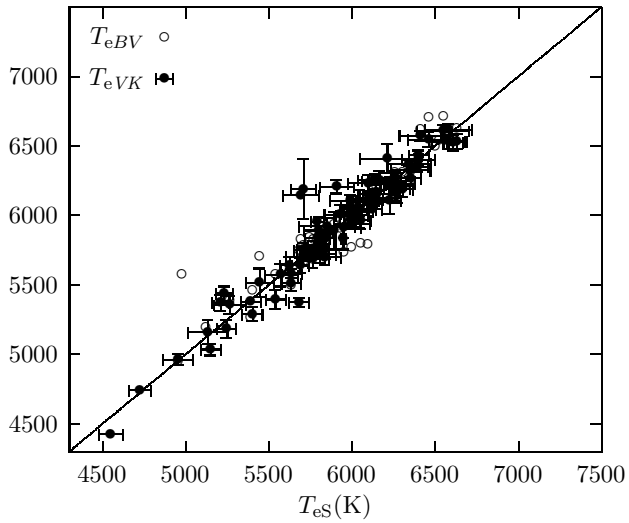

Figure 2. Effective temperatures of the target stars derived from fitting model colours to the observed colours $B-V$ ($T_{\rm eBV}$) and $V-K$ ($T_{\rm eVK}$) are plotted with respect to $T_{\rm eS}$.

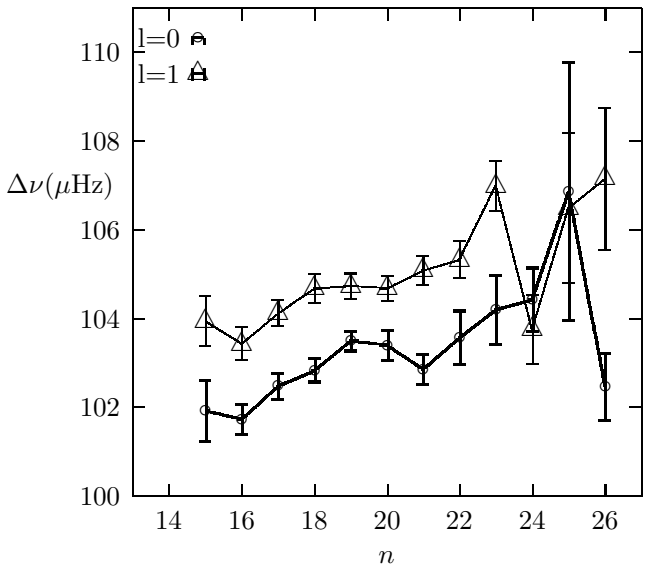

Figure 3. $\Delta\nu$ is plotted with respect to order n for the observed oscillation frequencies of 16 Cyg A (Metcalfe et al. 2012). The circle and triangle show the modes with $l=0$ and $l=1$, respectively. $\Delta\nu$ for $l=1$ is shifted up 1.25 μHz for a clear appearance. Two minima appear for $l=0$; one is about $n=16$ and the other is about $n=21$. Notice that there are large scattering for the modes with $n>23$. A similar scattering is seen in the early helioseismic data (see e.g. Grec, Fossat & Pomerantz 1983).

respectively. In Fig. 2, these effective temperatures are plotted with respect to $T_{\rm eS}$. The three effective temperatures are in good agreement. Only in the case of two stars, namely KIC 10920273 and HD 146233, there is a large difference between $T_{\rm eVK}$ and $T_{\rm eS}$. For most stars, the difference between $T_{\rm eVK}$ and $T_{\rm eS}$, $\delta T_{\rm eVK}=T_{\rm eVK}-T_{\rm eS}$, is as -100 K $<\delta T_{\rm eVK}<100$ K; few are out of this range. The results for $T_{\rm eBV}$, -150 K $<\delta T_{\rm eBV}<150$ K, are similar, showing that $T_{\rm eVK}$ is in better agreement with $T_{\rm eS}$ than $T_{\rm eBV}$.

We have already confirmed the presence of $\nu_{\rm min1}$ and $\nu_{\rm min2}$ in the observed oscillation frequencies of the Sun (BiSON data; Chaplin et al. 1999). It was unexpected to find two such minima in the oscillation frequencies of most of $Kepler$ and $CoRoT$ target stars. As an example $\Delta\nu$-n diagram of 16 Cyg A (Metcalfe et al. 2012) is plotted for degrees $l=0$ and 1 in Fig. 3. From data of both degrees, it was seen that minL corresponds to the mode with order $n=16$. The order of the minima with high frequency for $l=0$ is 21, and 20 for $l=1$.

In Fig. 4, $\nu_{\rm minH}$ and $\nu_{\rm minL}$ from the observed oscillation frequencies of the target stars are plotted with respect to $\nu_{\rm max}$. The most striking result is that for most, $\nu_{\rm minH}$ is greater than $\nu_{\rm max}$ while $\nu_{\rm minL}$ is lower than $\nu_{\rm max}$. For the ANKİ models (Paper I and II), the situation was found to be different: $\nu_{\rm min1}$ is less than $\nu_{\rm max}$ if $M<1.2{\rm M}_\odot$, otherwise $\nu_{\rm min1}>\nu_{\rm max}$. This inconsistency may arise from mismatch of the minima, i.e. minH may not be min1, and similarly min2 may not be minL. Another possibility is that the ordering of these frequencies according to their values is model dependent (see below).

In $\Delta\nu$-ν graph for the ANKİ models (see figure 3 of Paper I), the depth around $\nu_{\rm min1}$ is deeper than that of around $\nu_{\rm min2}$ for 1.0 $M_\odot$ models, and comparable to that of $\nu_{\rm min2}$ for 1.2 $M_\odot$ models. We notice considerable difference in the depths of minH and minL in $\Delta\nu$-ν graph for observed oscillation frequencies. The depth of minH is in general much shallower than that of minL. In figure 3 of Paper I, very clear shallow minima are seen in the high frequency ($\nu>\nu_{\rm min1}$) range for the models with 1.1 and 1.2 $M_\odot$.

Although the solar models constructed by using the ANKİ code are in good agreement with the helioseismic data of the Sun, there are significant differences between asteroseismic data of the solar-like oscillating stars and models, at least for $\nu_{\rm min1}$, $\nu_{\rm min2}$ and $\nu_{\rm max}$. Therefore, we construct new models using a different code, to make a comparison between their asteroseismic properties and the observed ones.

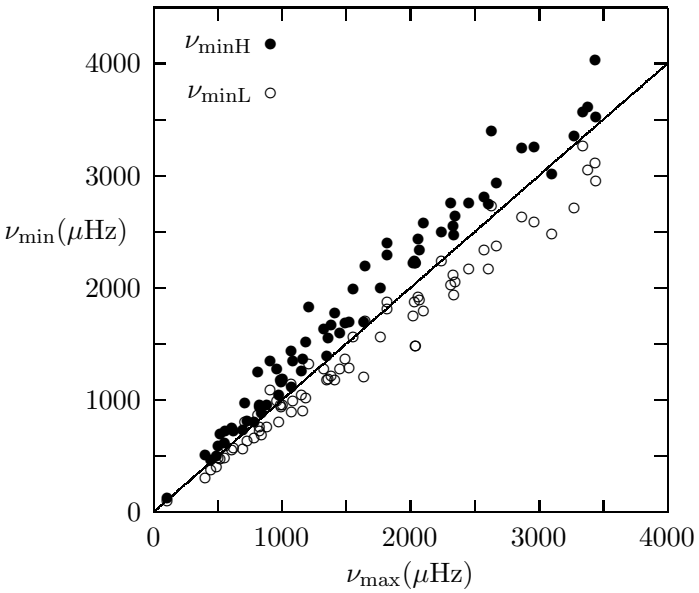

Figure 4. $\nu_{\rm minH}$ (filled circles) and $\nu_{\rm minL}$ (circles) of the observed frequencies are plotted with respect to $\nu_{\rm max}$.

3 PROPERTIES OF MESA MODELS AND ROLE OF Γ_{1S} IN SCALING RELATIONS

Our results presented in Paper I and II are based on the ANKİ models. It is important to test whether these results are code dependent. Furthermore, as emphasized above, there are large differences between models and the observed oscillation frequencies in terms of the relations between $\nu_{\rm max}$ and frequencies of minima. Therefore, we construct models by using the MESA evolution code (Paxton et al. 2011, 2013). As in the case of the ANKİ models, we obtain solar values by fitting interior model to the Sun, then use these values to construct stellar models. The solar values for the MESA code for initial hydrogen abundance (X), Z and the mixing-length parameter (α) are $X = 0.70358$, $Z = 0.0172$ and $\alpha = 2.175$. As in the case of the ANKİ models, we also construct models by using MESA for the mass range 0.8 $M_\odot \leqslant M \leqslant$ 1.6 $M_\odot$ and compute their adiabatic oscillation frequencies when the central hydrogen abundance ($X_{\rm c}$) is approximately $X_{\rm c} = 0.7$, 0.53, 0.35 and 0.17.

In the construction of interior models with MESA, standard mixing-length theory (Böhm-Vitense 1958) was derived for convection treatment, whereas the effects of convective overshooting were not considered. MESA *EOS* tables were selected for equation-of-state, and OPAL opacity tables (Iglesias & Rogers 1993, 1996) were used in the high temperature region supplemented by the low-temperature tables of Ferguson et al. (2005). Nuclear reaction rates were taken from Angulo et al. (1999) with significant updates (Kunz et al. 2002; Cyburt et al. 2010). The element diffusion is used in MESA default option (see in detail Paxton et al. 2011) for the solar model only. As stellar atmosphere, we choose `simple_photosphere` in our models. Adiabatic oscillation frequencies were computed using ADIPLS oscillation package (Christensen-Dalsgaard 2008) in the MESA module.

It is important first to clarify which of the minima found in observed oscillation frequencies ($\nu_{\rm minH}$ and $\nu_{\rm minL}$) matches min1 or min2. In Fig. 5, both model (min1 and min2) and observed (minH and minL) frequencies of minima are plotted with respect to $\nu_{\rm max}$. We notice that while $\nu_{\rm min1}$ and $\nu_{\rm min2}$ do not exactly match $\nu_{\rm minH}$ and $\nu_{\rm minL}$, $\nu_{\rm minL}$ and $\nu_{\rm min1}$ are in good agreement for the majority of the data. Revisiting the $\Delta\nu$-ν graph of some models, we find the frequencies of shallower minima (see e.g. fig. 3 in Paper I). Frequencies ($\nu_{\rm min0}$) of these minima (called as min0, in accordance with min1 and min2) are also plotted in Fig. 5. We confirm that $\nu_{\rm minH}$ corresponds $\nu_{\rm min0}$, for most of the stars.

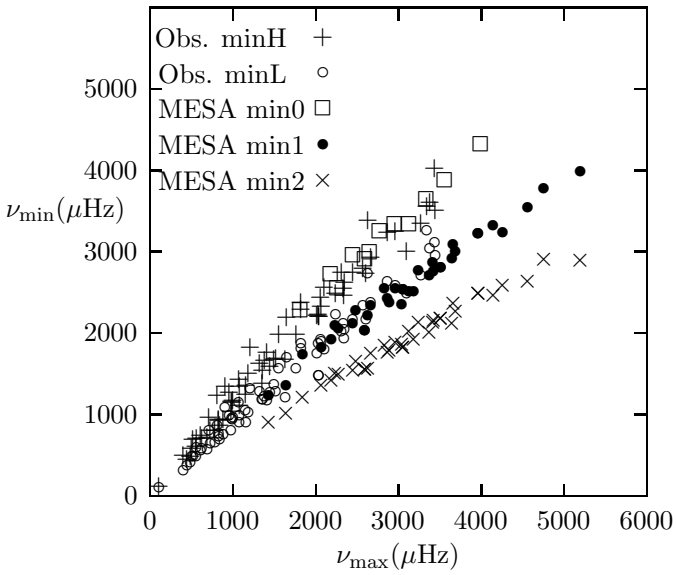

Figure 5. Comparison of model and observational frequencies of minima in $\Delta\nu$-ν graph. + and circle show observed oscillation frequencies of minH and minL, respectively. Square, filled circle and cross are for min0, min1 and min2 of model frequencies, respectively.

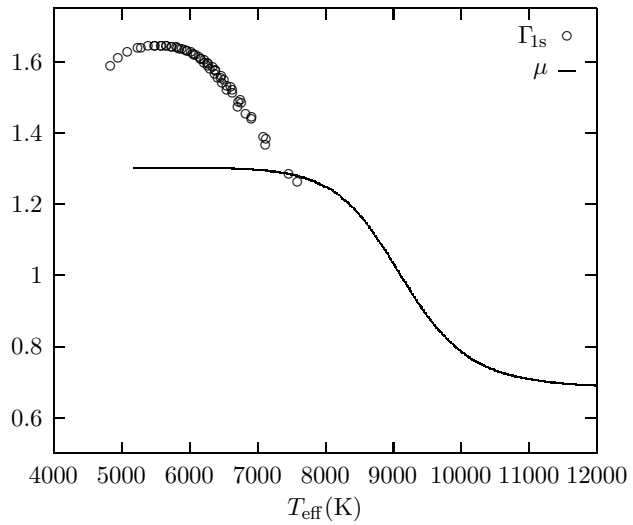

Figure 6. Γ_{1s} (circle) and μ (line) at the surface of interior models with respect to $T_{\rm eff}$.

3.1 Why Γ_{1s} is important in scaling relations?

In asteroseismic studies, $\nu_{\rm max}$ (Brown et al. 1991) is taken as

$$\nu_{\rm max} \propto \frac{g}{\sqrt{T_{\rm eff}}}. \quad (1)$$

$\nu_{\rm max}$ is assumed to be proportional to $\nu_{\rm ac}$ (Lamb 1909; Balmforth & Gough 1990), given as

$$\nu_{\rm ac} \sim \frac{c}{H}\left(1 - \frac{dH}{dr}\right), \quad (2)$$

where c and H are sound speed and pressure scale height at the stellar surface, respectively. dH/dr, gradient of H, has order about 10^{-4} and henceforth is negligibly small. If we insert the usual expressions for c and H in equation (2), we obtain

$$\nu_{\rm ac} = \frac{g}{\sqrt{\Re T_{\rm eff}}}\sqrt{\Gamma_{1s}\mu}. \quad (3)$$

where $\Re$ is the multiplication of Boltzmann constant and Avagadro's number. It is clear that equation (1) is valid if Γ_{1s} and μ are constant for the solar-like oscillating stars. We confirm below that this is the case.

In Fig. 6, Γ_{1s} and μ at the surface of interior models are plotted with respect to $T_{\rm eff}$. For the cool stars, both hydrogen and helium are neutral and μ is about 1.3. μ decreases as hydrogen and helium are ionized. For the solar-like oscillating stars ($T_{\rm eff} < 6900$ K), μ is constant in great extent. However, this is not the case for Γ_{1s}. Its maximum value is about 1.64 at about $T_{\rm eff} = 5500$ K and it decreases for higher or lower $T_{\rm eff}$ values. The value of Γ_{1s} for the hottest solar-like oscillating stars is 1.25, nearly 30 per cent below the maximum value. Therefore, to improve the accuracy of the scaling relation, it is important to take into account variation of Γ_{1s}.

Γ_{1s} is a function of $T_{\rm eff}$. We fit a parabolic function for $1/\Gamma_{1s}$

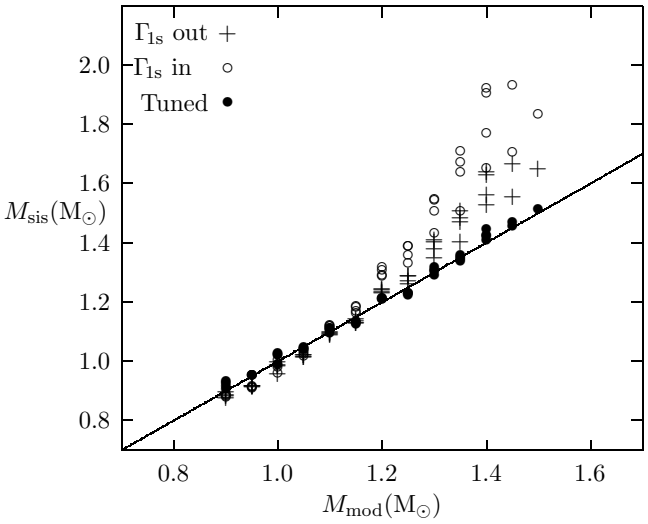

Figure 7. Comparison of asteroseismic masses computed from the customary scaling relation (+) and the new scaling relation (equation 5) with Γ_{1s} (circle). M_{sca} is plotted with respect to model mass in units of solar mass. For the tuned scaling relation (filled circle), see below (equation 9).

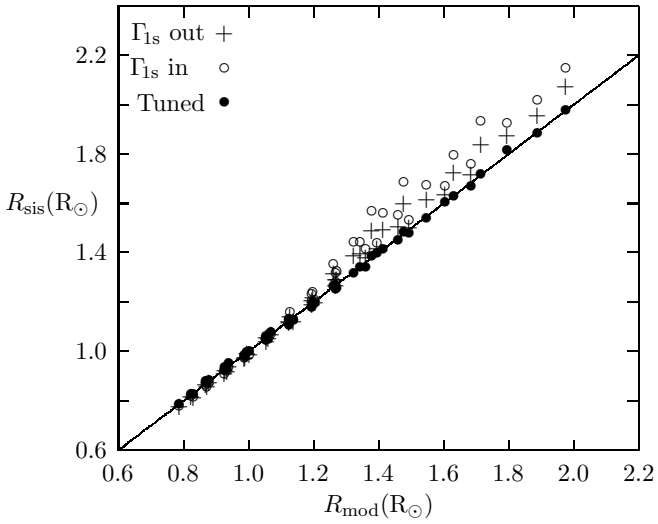

Figure 8. Comparison of asteroseismic radii computed from the customary scaling relation (+) and the new scaling relation (equation 6) with Γ_{1s} (circle). R_{sca} is plotted with respect to model radius in units of solar radius. For the tuned scaling relation (filled circle) for radius, see below (equation 10).

to the data shown in Fig. 6. The derived function is as

$$\frac{1}{\Gamma_{1s}} = 1.6\left(\frac{T_{\rm eff}}{T_{\rm eff\odot}} - 0.96\right)^2 + 0.607. \quad (4)$$

Equation (4) is very effective in representing Γ_{1s} for the cool stars in the ($T_{\rm eff}$) range under consideration in this study. For red giants, for example, there might be a deviation. If we adopt that Γ_{1s} is not constant, we obtain new scaling relations for stellar mass ($M''_{\rm sca}$) as

$$\frac{M''_{\rm sca}}{M_\odot} = \frac{(\nu_{\rm max}/\nu_{\rm max\odot})^3}{(\langle\Delta\nu\rangle\,/\,\langle\Delta\nu_\odot\rangle)^4}\left(\frac{T_{\rm eff}}{T_{\rm eff\odot}}\frac{\Gamma_{1s\odot}}{\Gamma_{1s}}\right)^{3/2} \quad (5)$$

and for radius ($R''_{\rm sca}$) as

$$\frac{R''_{\rm sca}}{R_\odot} = \frac{(\nu_{\rm max}/\nu_{\rm max\odot})}{(\langle\Delta\nu\rangle\,/\,\langle\Delta\nu_\odot\rangle)^2}\left(\frac{T_{\rm eff}}{T_{\rm eff\odot}}\frac{\Gamma_{1s\odot}}{\Gamma_{1s}}\right)^{1/2}. \quad (6)$$

In Fig. 7, $M''_{\rm sca}$ and mass from conventional scaling relation ($M'_{\rm sca}$) are plotted with respect to the model mass ($M_{\rm mod}$) in solar units. Despite the substantial difference between $M'_{\rm sca}$ and $M_{\rm mod}$ in particular for the models with $M > 1.2$ M$_\odot$, the inclusion of Γ_{1s} has the effect of increasing the difference, contrary to expectations.

We also test the scaling relation for stellar radius in Fig. 8, in which $R''_{\rm sca}$ and radius from conventional scaling relation ($R'_{\rm sca}$) are plotted with respect to $R_{\rm mod}$ in solar units. There is a significant difference between $R'_{\rm sca}$ and $R_{\rm mod}$ if $R > 1.2$ R$_\odot$, and the greater difference appears between $R''_{\rm sca}$ and $R_{\rm mod}$. This implies that the inclusion of Γ_{1s} in equation (3) itself does not result in improvement in scaling relations, highlighting the need for a much more general approach (see below).

$\Gamma_{1s\odot}$, the solar value of Γ_{1s}, is taken as 1.639. The other solar quantities used in equations (4)-(6) are given at the end of Table A1.

In scaling relations, we use $T_{\rm eS}$ in place of $T_{\rm eff}$. In our analysis, we use $T_{\rm eVK}$ for those seven stars for which no $T_{\rm eS}$ is available in the literature.

3.2 Tuning the scaling relations

It is reported in some studies (see e.g. White et al. 2011 and Sharma et al. 2016) that the relation between $\langle\Delta\nu\rangle$ and $\langle\rho\rangle^{1/2}$ deviates from a linear relation. In Fig. 9, the ratio of $\langle\Delta\nu\rangle\,/\,\langle\rho\rangle^{1/2}$ is plotted with respect to Γ_{1s} in solar units. There is a very clear linear relation between $\langle\Delta\nu\rangle\,/\,\langle\rho\rangle^{1/2}$ and Γ_{1s}. The fitting line is found as

$$\frac{\langle\Delta\nu\rangle\,/\,\langle\Delta\nu_\odot\rangle}{(\langle\rho\rangle\,/\,\langle\rho_\odot\rangle)^{1/2}} = f_{\Delta\nu} = 0.430\frac{\Gamma_{1s}}{\Gamma_{1s\odot}} + 0.570, \quad (7)$$

where $f_{\Delta\nu}$ is defined as the ratio $\langle\Delta\nu\rangle\,/\,\langle\rho\rangle^{1/2}$ in solar units. The range of $f_{\Delta\nu}$ is about [0.95,1.01]. In derivation of equation (7), we adopt $\langle\Delta\nu_\odot\rangle = 136$ μHz. Thus, we obtain its solar value as unity: $f_{\Delta\nu\odot} = 1$. There are two important indicators for $\langle\Delta\nu_\odot\rangle = 136$ μHz: i) The solar oscillation frequencies in Broomhall et al. (2009) yield the same value; ii) the maximum value of $\Delta\nu$ in between min1 and min2 is very close to 136 μHz. The latter point is important because this mode is the least effected, if not completely unaffected, by the He II ionization zone.

Understanding of the underlying physics of Γ_{1s} dependence of $\langle\Delta\nu\rangle\,/\,\langle\rho\rangle^{0.5}$ ratio can be achieved by comparing the solar model with a modified solar model (MSM). Suppose that Γ_{1s} in the most outer region of MSM is lower than $\Gamma_{1s\odot}$, otherwise identical to the solar model. In the outer region of MSM, sound travels more slowly than in the solar model. As speed is decreased in a part of the model, frequencies of all the modes decrease in accordence with the dispersion relation for sound waves. Radial nodes of MSM come to closer in the modified outer region and move away from each other in the unchanged interior regions. Although these two models have the same mean density, their oscillation frequencies are different. Oscillation frequency of MSM for a given mode (ν'_{nl}) is always less than that of the solar model ($\nu_{nl\odot}$): $\nu'_{nl} = q\nu_{nl\odot}$, where q is less than 1, depending on ratio of modified Γ_{1s} to $\Gamma_{1s\odot}$. Then, the large separation of MSM ($\Delta\nu'$) can be written as

$$\Delta\nu' = \nu'_{nl} - \nu'_{n-1,l} = q(\nu_{nl\odot} - \nu_{n-1,l\odot}) = q\Delta\nu_\odot.$$

This states that the ratio of $\Delta\nu'/\Delta\nu_\odot$ for the models with the same density is a function of the ratio ($\Gamma_{1s}/\Gamma_{1s\odot}$): $q = q(\Gamma_{1s}/\Gamma_{1s\odot})$.

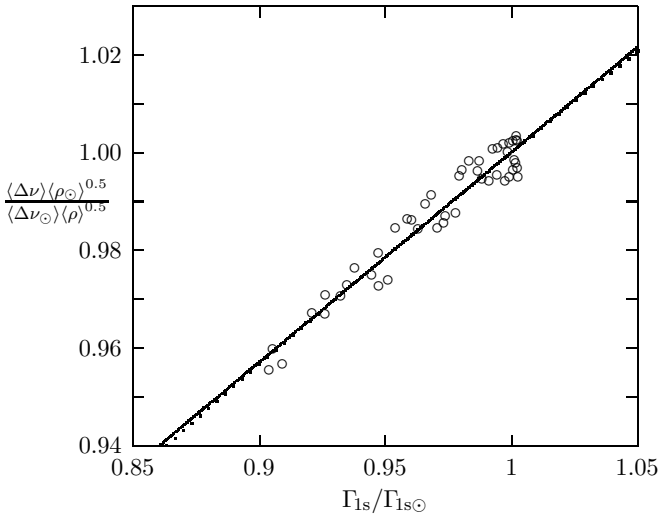

Figure 9. $\langle\Delta\nu\rangle\,/\,\langle\rho\rangle^{0.5}$ (in solar units) is plotted with respect to Γ_{1s}. The solid line is the fitted line $f_{\Delta\nu}=0.43\frac{\Gamma_{1s}}{\Gamma_{1s\odot}}+0.57$. The fitted curve (dotted line) is $\left(\frac{\Gamma_{1s}}{\Gamma_{1s\odot}}\right)^{0.42}$. These two functions are equivalent to each other.

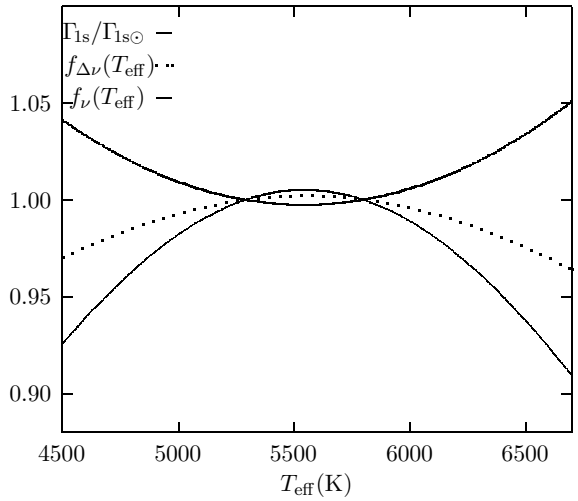

Figure 10. $\Gamma_{1s}/\Gamma_{1s\odot}$ (thin solid line), $f_{\Delta\nu}$ (dotted line) and f_ν (thick solid line) are plotted with respect to $T_{\rm eff}$. Around $T_{\rm eff}=5500$ K, they all are about unity.

We know that $\nu_{\rm ac}$ is also a function of Γ_{1s}. However, there is another underlying assumption for derivation of the scaling relations, which states that $\nu_{\rm ac}/\nu_{\rm max}$ is constant. However, it seems reasonable to assume that

$$\nu_{\rm max}=f_\nu\nu_{\rm ac}, \tag{8}$$

where f_ν is a parameter to be determined. Then, we derive new scaling relations for mass ($M_{\rm sca}$) and radius ($R_{\rm sca}$) as

$$\frac{M_{\rm sca}}{M_\odot}=\frac{(\nu_{\rm max}/\nu_{\rm max\odot})^3}{(\langle\Delta\nu\rangle\,/\,\langle\Delta\nu_\odot\rangle)^4}\left(\frac{T_{\rm eff}}{T_{\rm eff\odot}}\frac{\Gamma_{1s\odot}}{\Gamma_{1s}}\right)^{3/2}\frac{f_{\Delta\nu}^4}{f_\nu^3} \tag{9}$$

and

$$\frac{R_{\rm sca}}{R_\odot}=\frac{(\nu_{\rm max}/\nu_{\rm max\odot})}{(\langle\Delta\nu\rangle\,/\,\langle\Delta\nu_\odot\rangle)^2}\left(\frac{T_{\rm eff}}{T_{\rm eff\odot}}\frac{\Gamma_{1s\odot}}{\Gamma_{1s}}\right)^{1/2}\frac{f_{\Delta\nu}^2}{f_\nu}, \tag{10}$$

respectively. If we plot f_ν in equation (9) by taking $M_{\rm sca}=M_{\rm mod}$, we find a linear relation between f_ν and $\Gamma_{1s\odot}/\Gamma_{1s}$:

$$f_\nu=0.470\frac{\Gamma_{1s\odot}}{\Gamma_{1s}}+0.530. \tag{11}$$

If we plot f_ν in equation (10) by taking $R_{\rm sca}=R_{\rm mod}$, we find a very similar f_ν: $f_\nu=0.456\Gamma_{1s\odot}/\Gamma_{1s}+0.543$. In our computations, equation (11) is used for f_ν. The maximum difference between $R_{\rm sca}$ (equation 10) and $R_{\rm mod}$ is about 1 per cent if f_ν is taken as in equation (11). The maximum difference between $M_{\rm sca}$ (equation 9) and $M_{\rm mod}$ is about 2 per cent. The range of f_ν is about [0.94,1.0].

This indicates that Γ_{1s} is a hitherto neglected, but key factor in determining relations between asteroseismic and non-asteroseismic quantities. The parameters $f_{\Delta\nu}$ and f_ν, appearing in new scaling relations, are plotted in Fig. 10 with respect to $T_{\rm eff}$. We insert expression (4) for Γ_{1s} in equations (7) and (11). This gives expressions for $f_{\Delta\nu}$ and f_ν as functions of $T_{\rm eff}$. We notice that Γ_{1s}, $f_{\Delta\nu}$ and f_ν are approximately unity for the range 5200-5800 K. Outside this range, all deviate from unity, making conventional scaling relations much more uncertain.

$M_{\rm sca}$ and $R_{\rm sca}$ computed from equations (9) and (10) are also plotted in Figs. (7) and (8), respectively. Both of $M_{\rm sca}$ and $R_{\rm sca}$ are in very good agreement with model values.

Uncertainty in $M_{\rm sca}$ can be computed from uncertainties in $\nu_{\rm max}$, $\Delta\nu$ and $T_{\rm eff}$:

$$\frac{\Delta M_{\rm sca}}{M_{\rm sca}}=3\frac{\Delta\nu_{\rm max}}{\nu_{\rm max}}+4\frac{\Delta\,\langle\Delta\nu\rangle}{\langle\Delta\nu\rangle}+1.5\frac{\Delta T_{\rm eff}}{T_{\rm eff}}. \tag{12}$$

Similarly, uncertainty in radius can be obtained from

$$\frac{\Delta R_{\rm sca}}{R_{\rm sca}}=\frac{\Delta\nu_{\rm max}}{\nu_{\rm max}}+2\frac{\Delta\,\langle\Delta\nu\rangle}{\langle\Delta\nu\rangle}+0.5\frac{\Delta T_{\rm eff}}{T_{\rm eff}}. \tag{13}$$

$\Delta M_{\rm sca}$ and $\Delta R_{\rm sca}$ are computed for the target stars are given in the second row of the two lines for each star in Table A1.

3.3 $T_{\rm eff}$ from model frequencies

In Paper I, for the first time, ANKİ models were used to derive a relation between $T_{\rm eff}$ and $\Delta n_{x1}=(\nu_{\rm max}-\nu_{\rm min1})/\langle\Delta\nu\rangle$. Now we compute $\nu_{\rm max}$ of the MESA models not from equation (1) but from the following new relation

$$\frac{\nu_{\rm max}}{\nu_{\rm max\odot}}=f_\nu\left(\frac{T_{\rm eff\odot}}{T_{\rm eff}}\frac{\Gamma_{1s}}{\Gamma_{1s\odot}}\right)^{1/2}\frac{g}{g_\odot}. \tag{14}$$

For the MESA models, the relation between $T_{\rm eff}$ and Δn_{x1} is plotted in Fig. 11. From this relation, we obtain

$$\frac{T_{\rm sis1}(\Delta n_{x1})}{\rm T_{eff\odot}}=1.157-1.093\times10^{-9}(\Delta n_{x1}+15)^{6.4}. \tag{15}$$

The maximum difference between $T_{\rm sis1}$ from equation (15) and model $T_{\rm eff}$ is generally less than 100 K.

Similarly, we derive fitting formula for effective temperatures in terms of min0 ($T_{\rm sis0}$) and min2 ($T_{\rm sis2}$) frequencies (see Fig. 11), more precisely, $\Delta n_{x0}=(\nu_{\rm max}-\nu_{\rm min0})/\langle\Delta\nu\rangle$ and $\Delta n_{x2}=(\nu_{\rm max}-\nu_{\rm min2})/\langle\Delta\nu\rangle$;

$$\frac{T_{\rm sis0}(\Delta n_{x0})}{\rm T_{eff\odot}}=1.127-3.339\times10^{-9}(\Delta n_{x0}+20)^6 \tag{16}$$

and

$$\frac{T_{\rm sis2}(\Delta n_{x2})}{\rm T_{eff\odot}}=1.179-4.049\times10^{-9}(\Delta n_{x2}+10)^6. \tag{17}$$

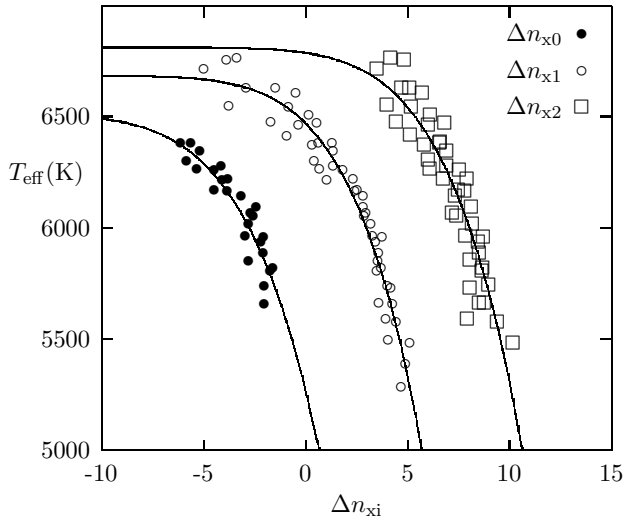

Figure 11. Effective temperature is plotted with respect to $\Delta n_{\rm x0}$ (filled circles), $\Delta n_{\rm x1}$ (circles) and $\Delta n_{\rm x2}$ (squares). The fitting curves are given in equations (15)-(17).

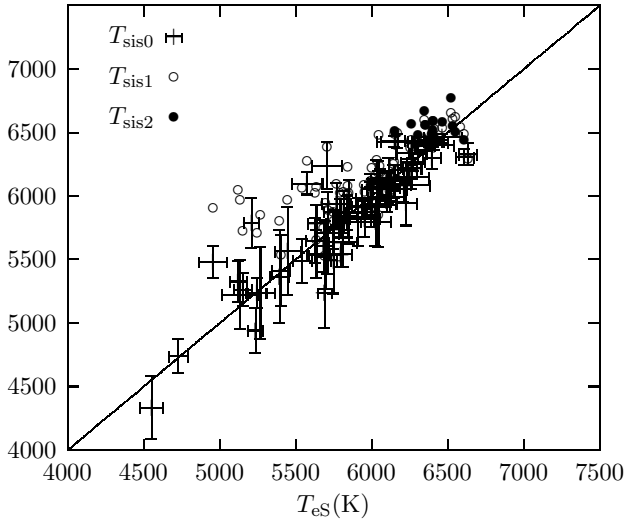

Figure 12. Effective temperatures of the target stars obtained by using oscillation frequencies are plotted with respect to $T_{\rm eS}$.

Expression for typical uncertainty in $T_{\rm sis0}$ can be obtained from equation (16) as

$$\frac{\Delta T_{\rm sis0}}{T_{\rm eff\odot}} = 2.0 \times 10^{-8} (\Delta n_{\rm x0} + 20)^5 \frac{\Delta\nu_{\rm max} + \Delta\nu_{\rm min0}}{\langle\Delta\nu\rangle}. \quad (18)$$

In a similar manner, expressions for uncertainties in $T_{\rm sis1}$ and $T_{\rm sis2}$ are derived from equations (15) and (17), respectively.

4 RESULTS AND DISCUSSIONS

4.1 Effective temperatures of the target stars

In the previous section, effective temperature was shown to be a function of order difference between the minima in $\Delta\nu$-ν graph and $\nu_{\rm max}$. Computations of $T_{\rm sis0}$, $T_{\rm sis1}$ and $T_{\rm sis2}$ of the target stars using equations (15)-(17) are listed in Table A1. $T_{\rm sis0}$, $T_{\rm sis1}$ and $T_{\rm sis2}$ are plotted with respect to $T_{\rm eS}$ in Fig. 12. In general, there is a very close agreement between asteroseismic $T_{\rm eff}$s ($T_{\rm sis0}$, $T_{\rm sis1}$ and $T_{\rm sis2}$) and $T_{\rm eS}$. However, a discrepancy occurs between $T_{\rm eS}$ and $T_{\rm sis1}$ in the case where $T_{\rm eS} < 5500$ K. min2 is only seen in $\langle\Delta\nu\rangle$-ν graph of very hot solar-like oscillating stars. Therefore, it was only possible to find $T_{\rm sis2}$ for 15 stars.

For some stars, there is a systematic difference between asteroseismic and non-asteroseismic $T_{\rm eff}$s. In some cases, such as KIC 3427720, KIC 3544595 and KIC 5866724, $T_{\rm eS}$ is greater than both $T_{\rm sis0}$ and $T_{\rm sis1}$, therefore, the the values of $\nu_{\rm max}$ should be decreased to fit $T_{\rm sis0}$ to $T_{\rm eS}$. For some targets (for example KIC 3424541, KIC 6679371 and KIC 7799349), however, $T_{\rm eS}$ is less than both of $T_{\rm sis0}$ and $T_{\rm sis1}$. In this case, $\nu_{\rm max}$ might be increased to fit $T_{\rm sis0}$ to $T_{\rm eS}$. This method will be considered in the next paper of this series.

For the Sun, the results are very impressive; the mean effective temperature from min0, min1 and min2 was obtained as 5804 ± 60 K. This value is very close to observed effective temperature of the Sun (5777 K), with very low standard deviation. Since there is no calibration of asteroseismic relations for effective temperature (equations 15-17), this finding alone shows the great value of asteroseismic tools.

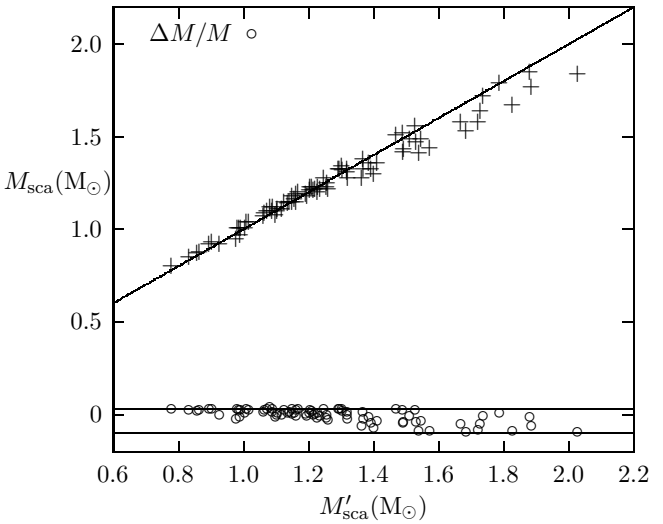

Figure 13. Mass of target stars computed by using the tuned scaling relation (equation 9) is plotted with respect to mass from the conventional scaling relation.

4.2 Masses and radii

In Fig. 13, $M_{\rm sca}$ ((equation 9)) is plotted with respect to $M'_{\rm sca}$. Also shown in Fig. 13 is the fractional difference between $M_{\rm sca}$ and $M'_{\rm sca}$. The horizontal solid lines are for 0.03 and -0.10. For $M < 1.3$ M$_\odot$, $M_{\rm sca}$ is nearly 3 per cent greater than $M'_{\rm sca}$. For $M > 1.3$ M$_\odot$; however, the difference between $M_{\rm sca}$ and $M'_{\rm sca}$ does not rise above 10 per cent.

$M_{\rm sca}$, $M'_{\rm sca}$, $R_{\rm sca}$ and $R'_{\rm sca}$ are listed in Table A1, together with the masses ($M_{\rm lit}$) and radii ($R_{\rm lit}$) of the target stars compiled from the literature. $M_{\rm lit}$ and $R_{\rm lit}$ were found by constructing interior models of the target stars, except Procyon A. The mass and radius of Procyon A given in Table A1 were obtained from observations (see Section 4.3). In Fig. 14, fractional mass difference between mass found from new scaling relation and mass from the literature, $\Delta M/M = (M_{\rm lit} - M_{\rm sca})/M_{\rm sca}$, is plotted with respect to fractional radius difference, $\Delta R/R = (R_{\rm lit} - R_{\rm sca})/R_{\rm sca}$. This figure shows that the maximum difference between $R_{\rm sca}$ and $R_{\rm lit}$

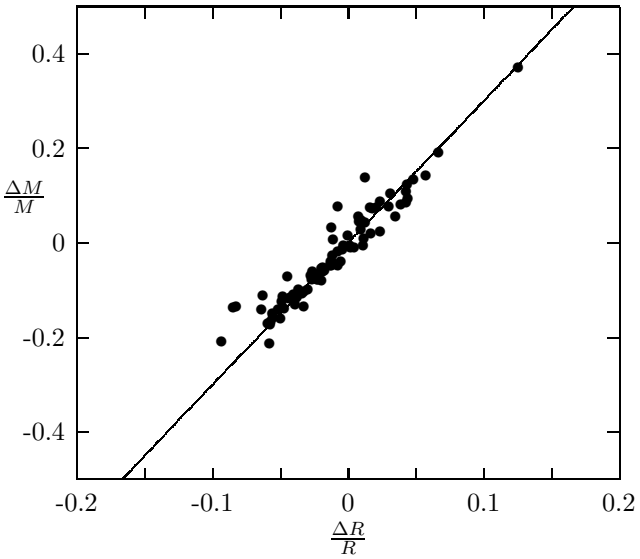

Figure 14. Fractional mass difference is plotted with respect to fractional radius difference. The solid line represents $\Delta M/M = 3\Delta R/R$.

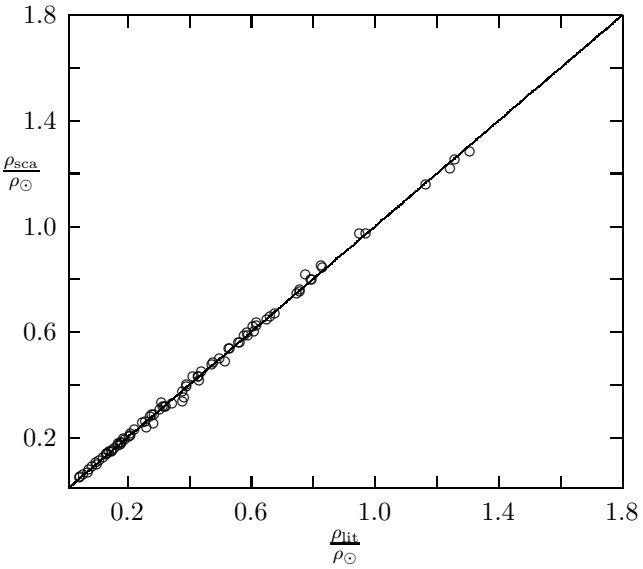

Figure 15. $\rho_{\rm sca}$ is plotted with respect to $\rho_{\rm lit}$.

is about 10 per cent, and is about 25 per cent for the mass. More crucially, it can be seen that there is a linear relation between the fractional mass and radius: $\Delta M/M = 3\Delta R/R$, imlpying that the density of the models are the same as that of given by $M_{\rm sca}/R^3_{\rm sca}$. This result arises from the fact that oscillation frequency of a given mode depends on mean stellar density, and may imply that density is indeed the fitted parameter in the calibration process of model frequencies to the observed oscillation frequencies. In that case, it is possible that different combinations of M and R yield the same density. In Fig. 15, $\rho_{\rm sca}/\rho_\odot = M_{\rm sca}/R^3_{\rm sca}$ is plotted with respect to $\rho_{\rm lit}/\rho_\odot = M_{\rm lit}/R^3_{\rm lit}$ (masses and radii are in solar units). Despite the significant differences between the masses and the radii (Fig. 14), the densities $\rho_{\rm sca}$ and $\rho_{\rm lit}$ are in very good agreement. Therefore, our further research will address the need for further constraints, such as frequencies of minimum $\Delta\nu$, when applying asteroseismic methods for finding fundamental properties of stars.

4.3 Comparison with masses and radii from non-asteroseismic measurements

Asteroseismic and non-asteroseismic effective temperatures of the Sun are compared above. Among the stars focused on, Procyon A is only star for which mass and radius are found by non-asteroseismic methods. Its mass was obtained by Bond et al. (2015) as 1.478 ± 0.012 $M_\odot$, and its radius was found as 2.03 ± 0.013 $R_\odot$ (Aufdenberg, Ludwig & Kervella, 2005). Conventional scaling relations give mass and radius as 1.63 $M_\odot$ and 2.14 $R_\odot$, respectively. Results from the new scaling relations for these two quantities are 1.46 $M_\odot$ and 2.03 $R_\odot$, respectively, very close to the observed values, showing the effectiveness of these new relations.

Another non-asteroseismic observational result for testing asteroseismic methods of the present study pertains to HD 181907. Its radius, found by interferometric methods, is 12.1 ± 0.5 $R_\odot$ (Baines et al. 2014), and its literature value is 12.93 ± 0.95 $R_\odot$ (Ghezzi & Johnson 2015). The old and new scaling relations, however, yield 12.91 and 12.42 $R_\odot$, respectively. Again, the radius from the new scaling relation is in very good agreement with the interferometric radius.

5 CONCLUSIONS

Asteroseismology of solar-like oscillating stars provides information about fundamental properties of these stars through the scaling relations. In these relations it is assumed that the first adiabatic exponent $\Gamma_{1\rm s}$ is constant. However, analysis of our models constructed by the MESA code shows that $\Gamma_{1\rm s}$ significantly changes through the surfaces of solar-like oscillating stars, depending on effective temperature. Furthermore, the ratio of the mean large separation $\langle\Delta\nu\rangle$ to $\langle\rho\rangle^{0.5}$, which is customarily assumed to be constant, is a linear function of $\Gamma_{1\rm s}$. Thus, it seems that $\Gamma_{1\rm s}$ is the factor in scaling relation that has previously been overlooked.

In contrast to the literature, we do not consider the ratios of $\nu_{\rm ac}/\nu_{\rm max}$ and $\nu_{\rm ac}/(g/T_{\rm eff}^{0.5})$ as constant. We show that these ratios can also be taken as functions of $\Gamma_{1\rm s}$. Then, we revise the scaling relations and obtain new relations for stellar mass and radius (equations 9 and 10), and then compute mass and radius of *Kepler* and *CoRoT* targets (89 stars + the Sun) using their asteroseismic properties. A difference of up to 10 per cent exists between the masses from new and old scaling relations. However, the great part of the uncertainties in mass and radius found from scaling relations comes from uncertainty in $\nu_{\rm max}$.

When mass and radius obtained from scaling relations are compared with those available in the literature, significant differences are seen. The fractional differences between the masses are up to $\Delta M/M = 0.25$ and $\Delta R/R = 0.10$. Particularly noteworthy, however, is the linear relation between $\Delta M/M$ and $\Delta R/R$: $\Delta M/M = 3\Delta R/R$ (see Fig. 14), highlighting that the fitted parameter is indeed mean density when oscillation frequencies of interior models are fitted to the observed oscillation frequencies.

We also computed effective temperatures of these stars using purely asteroseismic methods. In our previous paper (Paper I), the effective temperature of models was shown to be a function of $\Delta n_{\rm x1}$, which is approximately the order difference between the frequencies of maximum amplitude and min1 in the $\Delta\nu - \nu$ graph. Taking into account the effect of $\Gamma_{1\rm s}$, we derive new relations between $T_{\rm eff}$ and $\Delta n_{\rm x1}$ by using the MESA models. Similar expressions are obtained for $\Delta n_{\rm x0}$ and $\Delta n_{\rm x2}$. This allows us in principle to use three different methods to compute $T_{\rm eff}$ in terms of the

oscillation frequencies of the target stars. These effective temperatures ($T_{\rm sis0}$, $T_{\rm sis1}$ and $T_{\rm sis2}$; see equations 15-17) are in general in very good agreement within themselves and with $T_{\rm eff}$ from conventional methods. A significant difference appears between $T_{\rm sis1}$ and $T_{\rm eS}$ for cool stars, but not for the Sun, for example. The value of these new approaches lies in the increased number of methods they allow for computing the effective temperature of a solar-like oscillating star. The six methods consist of three asteroseismic, one spectroscopic and two photometric methods.

In principle, we can compute the fundamental stellar parameters by purely asterosesimic quantities, provided that the oscillation frequencies are precisely determined. The solar effective temperature is found as 5742, 5831 and 5840 K from frequencies of min0, min1 and min2, respectively. All of these values are very close to $T_{\rm eff\odot}$. Another key result we obtain is about Procyon A. Its mass is determined by using asterometric data from $Hubble\ Space\ Telescope$ as 1.478 ± 0.012 M$_\odot$. While the conventional scaling relation yields 1.63 M$_\odot$, the new scaling relation gives a much more accurate figure, 1.46 M$_\odot$.

However, in some cases, we confirm that there are systematic differences between asteroseismic and non-asteroseismic effective temperatures. These differences can be reduced or eliminated by increasing or decreasing $\nu_{\rm max}$. Such a modification, ciritical for obtaining more precise mass and radius from the scaling relations, will be the subject of our next paper.

ACKNOWLEDGEMENTS

Dr. Eric Michel is acknowledged for his discussions. This work is supported by the Scientific and Technological Research Council of Turkey (TÜBİTAK: 112T989).

REFERENCES

Angulo C. et al., 1999, Nucl. Phys. A, 656, 3
Appourchaux T. et al., 2008, A&A, 488, 705
Appourchaux T. et al., 2012, A&A, 543, A54
Appourchaux T. et al., 2014, A&A, 566, A20
Aufdenberg J. P., Ludwig H.-G., Kervella P., 2005, ApJ, 633, 424
Baglin A., Michel E., Auvergne M., COROT Team, 2006, in Fletcher K., ed., Proc. SOHO 18/GONG 2006/HELAS I, Beyond the Spherical Sun, Vol. 624, p. 34
Baines E. K., Armstrong J. T., Schmitt H. R., Benson J. A., Zavala R. T., van Belle G. T., 2014, ApJ, 781, 90
Ballard S. et al., 2014, ApJ, 790, 12
Ballot J. et al., 2011, A&A, 530, A97
Balmforth N. J., Gough D. O., 1990, ApJ, 362, 256
Barban C. et al., 2009, A&A, 506, 51
Bazot M. et al., 2012, A&A, 544, A106
Bedding T. R. et al., 2007, ApJ, 663, 1315
Bedding T. R. et al., 2010, ApJ, 713, 935
Belkacem K., Samadi R., Mosser B., Goupil M.-J., Ludwig H.-G., 2013, in Shibahashi H., Lynas-Gray A. E., eds, ASP Conf. Ser. Vol. 479, Progress in Physics of the Sun and Stars: A New Era in Helio- and Asteroseismology. Astron. Soc. Pac., San Francisco, p. 61
Benomar O., Masuda K., Shibahashi H., Suto Y., 2014, PASJ, 66, 94
Bond H. E. et al., 2015, ApJ, 813, 106
Borucki W. et al., 2010, Science, 327, 977
Boumier P. et al., 2014, A&A, 564, A34
Böhm-Vitense E., 1958, Zs. Ap., 46, 108
Brandão I. M. et al., 2011, A&A, 527, A37
Broomhall A. -M., Chaplin W. J., Davies G. R., Elsworth Y., Fletcher S. T., Hale S. J., Miller B., New R., 2009, MNRAS, 396, L100
Brown T. M., Gilliland R. L., Noyes R. W., Ramsey L. W., 1991, ApJ, 368, 599
Bruntt H. et al., 2010, MNRAS, 405, 1907
Bruntt H. et al., 2012, MNRAS, 423, 122
Campante T. L. et al., 2011, A&A, 534,A6
Carrier F. et al., 2010, A&A, 509, A73
Chaplin W. J., Miglio A., 2013, ARA&A, 51, 353
Chaplin W. J., Elsworth Y., Isaak G. R., Miller B. A., New R., 1999, MNRAS, 308, 424
Chaplin W. J. et al., 2013, ApJ, 766, 101
Chaplin W. J. et al., 2014, ApJS, 210, 1
Christensen-Dalsgaard J., 2002, RvMP, 74, 1073
Christensen-Dalsgaard J., 2008, Ap&SS, 316, 13
Christensen-Dalsgaard J., 2016, arXiv:1602.06838
Creevey O. L. et al., 2012, A&A, 537, A111
Cyburt R. H. et al., 2010, ApJS, 189, 240
Deheuvels S. et al., 2010, A&A, 515, A87
Deheuvels S., Michel E., 2011, A&A, 535, A91
Deheuvels S. et al., 2012, ApJ, 756, 19
Deheuvels S. et al., 2014, A&A, 564, A27
Doğan G. et al., 2013, ApJ, 763, 49
Eggenberger P., Carrier F., Bouchy F., Blecha A., 2004, A&A, 422, 247
Escobar M. E. et al., 2012, A&A, 543, A96
Ferguson J. W., Alexander D. R., Allard F., Barman T., Bodnarik J. G., Hauschildt P. H., Heffner-Wong A., Tamanai A., 2005, ApJ, 623, 585
Fuhrmann K., Preiffer M., Frank C., Reetz J, Gehren T., 1997, A&A, 323, 909
Gaulme P. et al., 2013, ApJ, 767, 82
García R. A. et al., 2014, A&A, 563, A84
García Hernández A., Martí-Ruiz S., Monteiro M. J. P. F. G., Suárez J. C., Reese D. R., Pascual-Granado J., Garrido R., 2015, ApJL, 811, L29
Ghezzi L., Johnson J. A., 2015, ApJ, 812, 96
Gilliland R. L. et al., 2013, ApJ, 766, 40
Grec G., Fossat E., Pomerantz M. A., 1983, SoPh, 82, 55
Hekker S., Ball W. H., 2014, A&A, 564, A105
Huber D. et al., 2011a, ApJ, 731, 94
Huber D. et al., 2011b, ApJ, 743, 143
Huber D. et al., 2013, ApJ, 767, 127
Iglesias C. A., Rogers, F. J., 1993, ApJ, 412, 752
Iglesias C. A., Rogers, F. J., 1996, ApJ, 464, 943
Kjeldsen H., Bedding T. R., 1995, A&A, 293, 87
Kosovichev A. G., 2011, in Lecture Notes in Physics, Vol. 832, ed. J.-P. Rozelot & C. Neiner (Berlin: Springer), p. 3
Kunz R., Fey M., Jaeger M., Mayer A., Hammer J. W., Staudt G., Harissopulos S., Paradellis T., 2002, ApJ, 567, 643
Lagarde N. et al., 2015, A&A, 580, A141
Lamb H., 1909, On the theory of waves propagated vertically in the atmosphere, Proc. London Math. Soc., 7, 122, 141
Lebreton Y., Goupil M. J., 2014, A&A, 569, A21
Lejeune T., Cuisinier F., Buser, R., 1998, A&AS, 130, 65
Li T. D., Bi S. L., Liu K., Tian Z. J., Shuai G. Z., 2012, A&A, 546, A83
Lillo-Box J. et al., 2014, A&A, 562, A109

Liu Z. et al., 2014, ApJ, 780, 152
Lund M. N., Kjeldsen H., Christensen-Dalsgaard J., Handberg R., Silva Aguirre V., 2014, ApJ, 782, 2
Marcy G. W. et al., 2014, ApJS, 210, 20
Mathur S. et al., 2012, ApJ, 749, 152
Metcalfe T. S. et al., 2012, ApJ, 748, L10
Metcalfe T. S. et al., 2014, ApJS, 214, 27
Molenda-Żakowicz J. et al., 2013, MNRAS, 434, 1422
Morel T., Rainer M., Poretti E., Barban C., Boumier P., 2013, A&A, 552, A42
Mortier A., Sousa S. G., Adibekyan V. Zh., Brandão I. M., Santos N. C., 2014, A&A, 572, A95
Mosser B. et al., 2008, A&A, 488, 635
Ozel N. et al., 2013, A&A, 558, A79
Paxton B. et al., 2011, ApJS, 192, 39
Paxton B. et al., 2013, ApJS, 208, 49
Ramírez I., Meléndez J., Cornejo D., Roederer I. U., Fish J. R., 2011, ApJ, 740, 76
Rawls M. L. et al., 2016, ApJ, 818, 108
Santos N. C. et al., 2013, A&A, 556, A150
Sharma S., Stello D., Bland-Hawthorn J., Huber D., Bedding T. R., 2016, arXiv:1603.05661
Soubiran C., Le Campion J.-F., Cayrel de Strobel G., Caillo A., 2010, A&A, 515, A111
White T. R., Bedding T. R., Stello D., Christensen-Dalsgaard J., Huber D., Kjeldsen H., 2011, ApJ, 743, 161
Yıldız M., 2015, RAA, 15, 2244
Yıldız M., Çelik Orhan Z., Aksoy Ç., Ok S., 2014, MNRAS, 441, 2148 (Paper I)
Yıldız M., Çelik Orhan Z., Kayhan C., 2015, MNRAS, 448, 3689 (Paper II)

APPENDIX A: BASIC ASTEROSEISMIC AND NON-ASTEROSEISMIC PROPERTIES OF *KEPLER* AND *COROT* TARGETS

Table A1: Basic properties of target stars. Columns are organized as star name, frequency of maximum amplitude, reference frequencies for min0, min1 and min2, mean large and small separations between oscillation frequencies, effective temperatures (from spectra, $V-K$ and $B-V$ colours (see Section 2) and from minima min0, min1 and min2 (see Section 3), respectively), masses and radii (from new and conventional scaling relations (see Section 3) and from literature, respectively), surface gravities (from new and conventional scaling relations (see Section 3), and from spectra, respectively), and numbers of references. Second row describes uncertainties of these basic properties. Unlike others, for Procyon A, mass and radius are the observed values, not the model values in the literature. Since $T_{\rm eS}$, $T_{\rm eVK}$ and $T_{\rm eBV}$ of KIC 11771760 are not available, we use $T_{\rm sis0}$ in scaling relations. The Sun is given at the end of the table.

Star	$\nu_{\rm max}$	$\nu_{\rm min0}$	$\nu_{\rm min1}$	$\nu_{\rm min2}$	$\langle\Delta\nu\rangle$	$\langle\delta\nu_{02}\rangle$	$T_{\rm eS}$	$T_{\rm eVK}$	$T_{\rm eBV}$	$T_{\rm sis0}$	$T_{\rm sis1}$	$T_{\rm sis2}$	$M_{\rm sca}$	$M'_{\rm sca}$	$M_{\rm lit}$	$R_{\rm sca}$	$R'_{\rm sca}$	$R_{\rm lit}$	$\log g_{\rm sca}$	$\log g'_{\rm sca}$	$\log g_{\rm spc}$	Ref
	μHz	μHz	μHz	μHz	μHz	μHz	K	K	K	K	K	K	$M_\odot$	$M_\odot$	$M_\odot$	$R_\odot$	$R_\odot$	$R_\odot$				
1435467	1324.0	1626.4	1274.0	—	70.9	4.8	6264	6224	6587	6217	6398	—	1.18	1.25	1.27	1.62	1.66	1.64	4.09	4.09	4.09	2,13,17
	39.7	16.3	12.7	—	0.8	—	60	51	185	82	87	—	0.18	0.18	0.05	0.09	0.09	0.03	0.01	0.01	0.03	39
2837475	1630.0	2265.6	1689.9	1276.8	75.2	6.7	6462	6545	6488	6464	6534	6575	1.75	1.93	1.39	1.76	1.85	1.59	4.19	4.19	3.95	2,17,39
	54.0	22.7	16.9	12.8	1.3	—	125	54	144	22	72	101	0.35	0.35	0.06	0.14	0.14	0.03	0.02	0.02	0.23	40
3424541	745.0	1046.6	755.4	—	41.1	4.7	6165	6249	6322	6431	6493	—	1.85	1.92	1.64	2.70	2.76	2.53	3.84	3.84	3.90	2,17,39
	55.0	10.5	7.6	—	1.1	—	108	73	249	56	137	—	0.65	0.65	0.04	0.37	0.37	0.07	0.02	0.02	0.21	40
3427720	2756.0	3044.3	2325.2	—	120.0	10.3	6040	6038	6055	5937	5845	—	1.27	1.30	1.13	1.17	1.19	1.13	4.40	4.40	4.38	2,13,17
	191.0	30.4	23.3	—	2.0	—	60	60	211	338	436	—	0.37	0.37	0.04	0.13	0.13	0.01	0.02	0.02	0.03	39
3544595	3366.0	3350.9	2702.9	—	145.5	8.7	5689	5640	5434	5237	5523	—	1.01	1.00	0.91	0.96	0.96	0.92	4.48	4.48	4.56	4,29,46
	81.0	33.5	27.0	—	1.5	—	48	52	200	280	225	—	0.13	0.13	0.06	0.05	0.05	0.02	0.01	0.01	0.06	
3632418	1159.0	1370.9	1055.0	—	60.4	3.8	6148	6154	6148	6122	6258	—	1.49	1.55	1.27	1.95	1.99	1.83	4.03	4.03	3.94	2,17,39
	44.0	13.7	10.6	—	0.4	—	111	38	77	126	139	—	0.25	0.25	0.03	0.12	0.12	0.03	0.01	0.01	0.21	40
3656476	1887.0	—	—	—	93.2	4.4	5710	5752	5303	—	—	—	1.06	1.05	1.09	1.31	1.31	1.32	4.23	4.23	4.23	13,17,37
	40.0	—	—	—	1.3	—	60	52	137	—	—	—	0.14	0.14	0.01	0.07	0.07	0.03	0.01	0.01	0.03	
3733735	1974.0	—	2211.0	1480.0	91.6	9.9	6548	6610	6581	—	6620	6499	1.42	1.59	1.32	1.43	1.52	1.37	4.28	4.28	3.99	2,17,39
	121.0	—	22.1	14.8	2.5	—	156	43	151	—	68	204	0.47	0.47	0.04	0.18	0.18	0.02	0.02	0.02	0.22	40
3735871	2633.0	2850.7	—	—	124.7	12.3	5908	6207	5908	5797	—	—	0.93	0.94	1.07	1.03	1.04	1.09	4.38	4.38	—	2,17
	79.0	28.5	—	—	3.3	—	100	49	202	189	—	—	0.21	0.21	0.12	0.09	0.09	0.05	0.02	0.02	—	
4349452	2106.0	2568.7	1884.4	—	97.6	7.7	6270	6194	6048	6267	6160	—	1.33	1.40	1.19	1.36	1.40	1.31	4.30	4.29	4.28	9,29,36
	50.0	25.7	18.8	—	1.0	—	79	107	—	69	125	—	0.17	0.17	0.06	0.07	0.07	0.02	0.01	0.01	0.03	
4914923	1849.0	1947.8	—	—	88.7	6.1	5808	5721	5910	5635	—	—	1.24	1.24	1.10	1.43	1.43	1.37	4.22	4.22	4.28	17,37,40
	46.0	19.5	—	—	0.3	—	92	65	194	192	—	—	0.14	0.14	0.01	0.06	0.06	0.05	0.01	0.01	0.21	
5184732	2068.0	2182.6	1705.5	—	95.1	5.9	5840	5836	5611	5660	5779	—	1.32	1.32	1.25	1.39	1.39	1.36	4.27	4.27	4.26	13,17,37
	47.0	—	18.8	—	1.3	—	60	41	91	—	113	—	0.18	0.18	0.01	0.08	0.08	0.01	0.01	0.01	0.03	
5512589	1224.0	—	—	—	68.2	5.5	5764	5687	5583	—	—	—	1.02	1.02	1.16	1.60	1.59	1.67	4.04	4.04	4.22	17,37,40
	43.0	—	—	—	0.7	—	95	64	203	—	—	—	0.17	0.17	0.01	0.10	0.10	0.01	0.01	0.01	0.21	
5607242	610.0	745.3	543.4	—	40.5	3.7	5572	5572	5070	6097	6270	—	0.97	0.96	1.33	2.22	2.21	2.49	3.73	3.73	—	2,17
	18.3	7.5	5.4	—	0.8	—	100	83	272	88	88	—	0.19	0.19	0.11	0.17	0.17	0.10	0.02	0.02	—	
5689820	695.0	—	—	—	41.0	3.9	4978	—	—	—	—	—	1.11	1.15	1.14	2.29	2.33	—	3.76	3.76	—	22
	15.0	—	—	—	0.5	—	167	—	—	—	—	—	0.18	0.18	—	0.14	0.14	—	0.01	0.01	—	
5866724	1880.0	2171.6	1674.4	—	89.6	6.6	6211	6410	5574	6085	6155	—	1.32	1.38	1.27	1.44	1.47	1.42	4.24	4.24	4.23	16,29
	60.0	21.7	16.7	—	0.9	—	167	104	369	130	153	—	0.23	0.23	0.06	0.09	0.09	0.02	0.01	0.01	0.01	
5955122	861.0	952.7	717.9	—	49.4	4.8	5952	5917	6068	5822	6026	—	1.33	1.35	1.12	2.16	2.17	2.04	3.89	3.89	4.13	2,17,39
	24.0	9.5	7.2	—	0.9	—	100	78	192	144	130	—	0.24	0.24	0.05	0.16	0.16	0.03	0.02	0.02	0.21	40
6106415	2260.0	2533.1	1909.2	—	103.9	6.5	5990	6056	6040	5980	5904	—	1.24	1.26	1.12	1.28	1.29	1.24	4.32	4.32	4.31	13,17,37
	53.0	25.3	19.1	—	0.3	—	60	50	76	129	161	—	0.12	0.12	0.02	0.04	0.04	0.01	0.01	0.01	0.03	

Table A1: – continued from previous page

Star	$\nu_{\rm max}$	$\nu_{\rm min0}$	$\nu_{\rm min1}$	$\nu_{\rm min2}$	$\langle\Delta\nu\rangle$	$\langle\delta\nu_{02}\rangle$	$T_{\rm eS}$	$T_{\rm eVK}$	$T_{\rm eBV}$	$T_{\rm sis0}$	$T_{\rm sis1}$	$T_{\rm sis2}$	$M_{\rm sca}$	$M'_{\rm sca}$	$M_{\rm lit}$	$R_{\rm sca}$	$R'_{\rm sca}$	$R_{\rm lit}$	$\log g_{\rm sca}$	$\log g'_{\rm sca}$	$\log g_{\rm spc}$	Ref
	μHz	μHz	μHz	μHz	μHz	μHz	K	K	K	K	K	K	$M_\odot$	$M_\odot$	$M_\odot$	$R_\odot$	$R_\odot$	$R_\odot$				
6116048	2020.0	2250.4	1748.1	—	100.5	5.9	5991	6109	5844	5916	6069	—	1.01	1.03	1.12	1.23	1.24	1.26	4.27	4.27	4.09	2,3,37
	60.6	22.5	17.5	—	0.2	—	124	41	119	156	154	—	0.13	0.13	0.02	0.06	0.06	0.01	0.01	0.01	0.22	40
6508366	926.0	1267.5	978.3	672.2	51.5	3.3	6354	6268	6414	6400	6548	6551	1.46	1.57	1.36	2.14	2.22	2.08	3.94	3.94	3.94	2,13,17
	36.0	12.7	9.8	6.7	0.8	—	60	60	177	43	64	101	0.28	0.28	0.04	0.16	0.16	0.02	0.01	0.01	0.03	39
6603624	2402.0	2529.7	2080.5	—	109.7	5.5	5625	5642	5364	5649	6017	—	1.12	1.11	1.09	1.20	1.19	1.18	4.33	4.33	4.32	2,13,17
	51.0	25.3	20.8	—	1.7	—	60	58	113	179	137	—	0.16	0.16	0.03	0.07	0.07	0.02	0.01	0.01	0.03	39
6679371	908.0	1284.8	1000.6	725.8	50.6	4.1	6344	6375	6453	6435	6591	6662	1.48	1.59	1.56	2.17	2.25	2.19	3.93	3.93	3.92	2,3,39
	27.2	12.8	10.0	7.3	0.7	—	131	21	132	26	41	57	0.26	0.26	0.03	0.15	0.15	0.02	0.01	0.01	0.21	40
6933899	1391.0	1538.7	1178.0	—	71.8	4.9	5837	5700	5982	5866	6009	—	1.24	1.24	1.14	1.64	1.64	1.60	4.10	4.10	4.21	2,17,39
	32.0	15.4	11.8	—	1.0	—	97	58	191	133	128	—	0.18	0.18	0.03	0.10	0.10	0.02	0.01	0.01	0.22	40
7103006	1124.0	1432.9	1134.4	790.3	60.1	4.5	6394	6351	6151	6302	6486	6480	1.41	1.53	1.43	1.90	1.98	1.90	4.03	4.03	4.01	2,13,17
	54.0	14.3	11.3	7.9	1.1	—	60	42	126	89	100	147	0.33	0.33	0.05	0.17	0.17	0.03	0.02	0.02	0.03	39
7106245	2323.0	—	2105.0	—	111.6	7.0	6000	6000	5725	—	6218	—	1.01	1.03	—	1.14	1.15	—	4.33	4.33	—	2
	69.7	—	21.0	—	1.1	—	99	98	479	—	133	—	0.16	0.16	—	0.07	0.07	—	0.01	0.01	—	
7206837	1592.0	2023.7	1545.1	1153.7	78.7	6.2	6304	6190	6480	6330	6411	6478	1.36	1.44	1.46	1.58	1.63	1.56	4.17	4.17	4.17	2,13,17
	70.0	20.2	15.5	11.5	1.4	—	60	60	263	80	124	149	0.29	0.29	0.05	0.13	0.13	0.02	0.02	0.02	0.03	39
7341231	408.0	384.5	—	—	28.8	3.4	5233	5440	5438	4941	—	—	1.03	1.03	0.90	2.84	2.84	2.69	3.54	3.54	3.54	2,17,21
	8.0	3.8	—	—	0.7	—	50	51	180	174	—	—	0.17	0.17	0.10	0.21	0.21	0.20	0.02	0.02	0.03	
7680114	1684.0	—	—	—	85.1	—	5799	5891	5588	—	—	—	1.10	1.10	1.19	1.41	1.41	1.45	4.18	4.18	4.25	17,37,40
	47.0	—	—	—	1.3	—	91	94	268	—	—	—	0.19	0.19	0.01	0.09	0.09	0.03	0.01	0.01	0.21	
7747078	936.0	1039.3	792.5	—	53.4	4.7	5840	5754	5727	5840	6074	—	1.23	1.24	1.06	2.00	2.00	1.89	3.93	3.93	3.91	2,13,17
	32.0	10.4	7.9	—	0.3	—	60	66	172	165	147	—	0.17	0.17	0.05	0.10	0.10	0.02	0.01	0.01	0.03	39
7799349	561.0	580.6	448.6	—	33.2	3.4	4954	4962	4821	5479	5902	—	1.34	1.39	1.39	2.80	2.86	—	3.67	3.67	3.33	2,22,40
	8.0	5.8	4.5	—	0.4	—	92	41	124	124	87	—	0.16	0.16	—	0.13	0.13	—	0.01	0.01	0.22	
7871531	3344.0	3403.0	2658.3	—	151.3	10.1	5400	5289	5641	5413	5533	—	0.78	0.78	0.84	0.86	0.86	0.87	4.46	4.46	4.49	2,13,39
	100.3	34.0	26.6	—	3.6	—	60	51	145	279	253	—	0.16	0.16	0.02	0.07	0.07	0.01	0.02	0.02	0.20	
7976303	851.0	1036.3	754.0	—	51.0	4.5	6053	5967	6315	6139	6228	—	1.15	1.17	1.17	2.00	2.03	2.03	3.89	3.89	3.87	13,17,37
	20.0	10.4	7.5	—	0.6	—	60	66	182	75	87	—	0.15	0.15	0.02	0.10	0.10	0.05	0.01	0.01	0.03	
8006161	3481.0	3518.3	2922.7	—	149.2	10.3	5390	5378	5189	5365	5800	—	0.93	0.93	1.00	0.92	0.92	0.93	4.48	4.48	4.49	2,13,17
	133.0	35.2	29.2	—	1.8	—	60	—	—	367	275	—	0.17	0.17	0.01	0.06	0.06	—	0.01	0.01	0.03	37
8026226	545.0	687.7	479.1	—	34.6	3.6	6230	6233	6204	6202	6227	—	1.45	1.53	1.50	2.80	2.87	2.75	3.71	3.71	3.71	2,13,17
	22.0	6.9	4.8	—	0.6	—	60	45	127	91	125	—	0.30	0.30	0.03	0.22	0.22	0.04	0.02	0.02	0.03	39
8219268	109.0	90.5	—	—	9.4	1.1	4550	4424	4702	4335	—	—	1.27	1.42	1.34	6.32	6.69	6.53	2.94	2.94	3.00	29,33
	3.3	0.9	—	—	0.1	—	75	—	—	248	—	—	0.20	0.20	0.17	0.37	0.37	0.35	0.01	0.01	0.30	
8228742	1171.0	1375.9	1036.9	—	62.0	4.8	6042	6048	6096	6093	6180	—	1.37	1.41	1.31	1.87	1.89	1.84	4.03	4.03	4.02	2,13,17
	34.0	13.8	10.4	—	0.6	—	60	56	206	108	124	—	0.19	0.19	0.01	0.10	0.10	0.01	0.01	0.01	0.03	37
8379927	2669.0	2981.4	2364.9	—	120.0	10.6	5998	5939	6096	5975	6107	—	1.15	1.17	1.09	1.13	1.14	1.11	4.39	4.39	4.25	2,3,37
	80.1	29.8	23.6	—	1.0	—	108	—	—	158	164	—	0.17	0.17	0.03	0.06	0.06	0.02	0.01	0.01	0.21	40
8394589	2165.0	2547.2	1891.5	—	109.5	8.1	6111	6105	5974	6120	6114	—	0.90	0.93	0.94	1.11	1.13	1.12	4.30	4.30	3.98	2,17,39
	124.0	25.5	18.9	—	1.9	—	116	74	260	181	245	—	0.24	0.24	0.04	0.11	0.11	0.02	0.02	0.02	0.21	40
8524425	1081.0	1128.0	831.3	—	59.4	5.0	5634	5513	5515	5541	5651	—	1.19	1.18	1.00	1.84	1.83	1.73	3.98	3.98	3.98	2,13,17
	28.0	11.3	8.3	—	0.6	—	60	57	188	187	171	—	0.16	0.16	0.07	0.09	0.09	0.02	0.01	0.01	0.03	39
8561221	491.0	488.0	370.5	—	29.8	2.4	5245	5183	5374	5238	5705	—	1.56	1.56	1.55	3.19	3.19	3.18	3.62	3.62	3.61	13,25
	5.0	4.9	3.7	—	0.1	—	60	62	199	118	79	—	0.10	0.10	0.13	0.08	0.08	0.18	0.01	0.01	0.03	
8694723	1384.0	1661.8	1261.7	—	74.9	5.4	6258	6230	6355	6149	6272	—	1.08	1.14	0.96	1.51	1.56	1.44	4.11	4.11	3.97	2,3,39
	41.5	16.6	12.6	—	0.8	—	117	36	137	96	109	—	0.17	0.17	0.03	0.09	0.09	0.02	0.01	0.01	0.21	40

Table A1: – continued from previous page

Star	$\nu_{\rm max}$	$\nu_{\rm min0}$	$\nu_{\rm min1}$	$\nu_{\rm min2}$	$\langle\Delta\nu\rangle$	$\langle\delta\nu_{02}\rangle$	$T_{\rm eS}$	$T_{\rm eVK}$	$T_{\rm eBV}$	$T_{\rm sis0}$	$T_{\rm sis1}$	$T_{\rm sis2}$	$M_{\rm sca}$	$M'_{\rm sca}$	$M_{\rm lit}$	$R_{\rm sca}$	$R'_{\rm sca}$	$R_{\rm lit}$	$\log g_{\rm sca}$	$\log g'_{\rm sca}$	$\log g_{\rm spc}$	Ref
	μHz	μHz	μHz	μHz	μHz	μHz	K	K	K	K	K	K	$M_\odot$	$M_\odot$	$M_\odot$	$R_\odot$	$R_\odot$	$R_\odot$				
8702606	664.0	688.7	554.5	—	39.7	3.5	5540	5396	5445	5489	6057	—	1.35	1.34	1.27	2.51	2.50	—	3.77	3.77	3.76	2,13,22
	16.0	6.9	5.5	—	0.5	—	60	70	192	171	108	—	0.19	0.19	—	0.14	0.14	—	0.01	0.01	0.03	
8760414	2384.0	2628.3	2041.6	—	117.1	5.6	5850	5925	5981	5873	6019	—	0.88	0.88	0.78	1.06	1.06	1.01	4.33	4.33	3.94	2,17,39
	121.0	26.3	20.4	—	0.4	—	166	59	194	251	252	—	0.18	0.18	0.01	0.08	0.08	0.01	0.01	0.01	0.26	40
9025370	2653.0	3246.7	2540.0	—	133.3	8.7	5704	5704	5630	6238	6381	—	0.70	0.70	0.84	0.90	0.90	0.96	4.37	4.37	—	2,17
	215.0	32.5	25.4	—	1.9	—	99	71	116	183	222	—	0.23	0.23	0.13	0.11	0.11	0.05	0.01	0.01	—	
9098294	2233.0	2494.9	1949.7	—	108.8	5.9	5766	5756	5930	5938	6092	—	0.96	0.96	1.00	1.14	1.14	1.15	4.30	4.30	4.27	2,17,39
	75.0	24.9	19.5	—	1.7	—	96	60	269	168	167	—	0.18	0.18	0.03	0.08	0.08	0.01	0.01	0.01	0.21	40
9139151	2610.0	2972.7	2270.0	—	116.7	10.1	6125	6116	6265	6062	6022	—	1.22	1.26	1.14	1.18	1.20	1.15	4.38	4.38	4.38	2,13,39
	78.3	29.7	22.7	—	2.1	—	60	53	214	138	180	—	0.22	0.22	0.03	0.08	0.08	0.01	0.02	0.02	0.03	
9139163	1608.0	2202.8	1619.8	1179.8	81.0	6.6	6400	6432	6395	6431	6484	6512	1.25	1.36	1.36	1.50	1.56	1.53	4.18	4.18	4.18	2,13,17
	58.0	22.0	16.2	11.8	1.1	—	60	36	128	34	85	115	0.22	0.22	0.03	0.10	0.10	0.02	0.01	0.01	0.03	39
9206432	1853.0	2289.7	1863.9	1355.8	84.3	7.7	6608	6524	6597	6306	6482	6433	1.63	1.86	1.40	1.58	1.69	1.48	4.25	4.25	4.23	2,13,17
	46.0	22.9	18.6	13.6	1.3	—	60	56	174	63	71	110	0.24	0.24	0.03	0.10	0.10	0.01	0.01	0.01	0.03	39
9410862	2261.0	2449.0	1912.1	—	107.0	7.8	6024	6024	6203	5799	5935	—	1.11	1.13	1.12	1.21	1.22	1.22	4.32	4.32	—	2,17
	67.8	24.5	19.1	—	1.9	—	100	118	—	189	183	—	0.21	0.21	0.11	0.09	0.09	0.05	0.02	0.02	—	
9574283	455.0	459.3	370.6	—	29.9	3.0	5120	—	—	5328	6044	—	1.16	1.18	1.07	2.88	2.90	—	3.59	3.59	—	2,17,22
	10.0	4.6	3.7	—	0.8	—	55	—	—	163	93	—	0.22	0.22	—	0.23	0.23	—	0.02	0.02	—	
9812850	1195.0	1558.0	1171.2	877.2	65.1	4.1	6258	6272	6393	6336	6436	6557	1.22	1.29	1.39	1.73	1.78	1.75	4.05	4.05	3.94	2,17,39
	60.0	15.6	11.7	8.8	1.1	—	97	51	223	78	118	126	0.29	0.29	0.05	0.16	0.16	0.02	0.02	0.02	0.21	40
9955598	3546.0	3530.0	2995.3	—	153.0	9.5	5264	5355	5480	5236	5842	—	0.85	0.85	0.89	0.88	0.88	0.88	4.48	4.48	4.29	2,29,39
	119.0	35.3	30.0	—	3.1	—	95	66	197	359	238	—	0.18	0.18	0.02	0.07	0.07	0.01	0.02	0.02	0.12	40
10018963	987.0	1168.7	866.0	—	55.2	5.1	6145	6125	6285	6091	6175	—	1.32	1.37	1.18	1.99	2.03	1.92	3.96	3.96	3.95	2,17,39
	32.0	11.7	8.7	—	0.5	—	112	43	131	111	128	—	0.21	0.21	0.03	0.12	0.12	0.02	0.01	0.01	0.21	40
10162436	968.0	1370.4	977.0	671.1	55.5	3.6	6149	6155	6397	6427	6485	6505	1.22	1.27	1.23	1.93	1.97	1.90	3.95	3.95	3.95	2,17,39
	49.0	13.7	9.8	6.7	0.7	—	115	—	—	41	98	136	0.28	0.28	0.02	0.16	0.16	0.02	0.01	0.01	0.21	40
10355856	1330.0	1823.7	1308.8	—	68.1	4.7	6351	6326	6490	6427	6441	—	1.41	1.52	1.32	1.76	1.82	1.67	4.10	4.10	3.93	2,17,39
	42.0	18.2	13.1	—	0.7	—	118	47	189	32	85	—	0.23	0.23	0.03	0.11	0.11	0.01	0.01	0.01	0.21	40
10454113	2261.0	2594.3	2019.3	—	103.8	8.6	6120	6044	6179	6078	6148	—	1.27	1.31	1.19	1.29	1.31	1.25	4.32	4.32	4.31	2,13,17
	62.0	25.9	20.2	—	1.3	—	60	—	144	122	143	—	0.19	0.19	0.04	0.07	0.07	0.01	0.01	0.01	0.03	39
10516096	1700.0	—	—	—	84.6	—	5928	6006	5775	—	—	—	1.19	1.20	1.12	1.45	1.46	1.42	4.19	4.19	4.24	17,37,40
	30.0	—	—	—	1.1	—	95	67	188	—	—	—	0.15	0.15	0.03	0.07	0.07	0.03	0.01	0.01	0.21	
10644253	2819.0	3234.8	2623.1	—	123.2	9.8	6030	6046	5932	6103	6279	—	1.22	1.25	1.13	1.14	1.15	1.11	4.41	4.41	4.40	2,13,17
	131.0	32.3	26.2	—	2.7	—	60	60	160	182	191	—	0.30	0.30	0.05	0.11	0.11	0.02	0.02	0.02	0.03	39
10909629	839.0	—	843.7	—	49.6	3.0	6046	6046	6133	—	6479	—	1.23	1.26	1.36	2.09	2.11	2.17	3.89	3.89	—	2,17
	37.0	—	8.4	—	1.0	—	99	137	—	—	86	—	0.29	0.29	0.11	0.19	0.19	0.07	0.02	0.02	—	
10920273	1024.0	1103.1	826.6	—	57.1	4.9	5710	6189	6725	5707	5882	—	1.20	1.20	1.00	1.90	1.89	1.78	3.96	3.96	4.15	14,18,23
	64.0	11.0	8.3	—	0.6	—	75	216	—	319	299	—	0.30	0.30	0.04	0.17	0.17	0.02	0.01	0.01	0.08	
10963065	2184.0	2497.9	1885.3	—	102.6	7.3	6097	6116	6177	6054	6023	—	1.19	1.23	1.05	1.27	1.29	1.21	4.30	4.30	4.00	2,17,39
	62.0	25.0	18.9	—	1.0	—	130	35	143	128	163	—	0.19	0.19	0.02	0.07	0.07	0.01	0.01	0.01	0.21	40
11026764	895.0	945.6	698.3	—	50.2	4.5	5682	5374	5727	5605	5746	—	1.33	1.32	1.27	2.14	2.13	2.11	3.90	3.90	3.88	2,13,17
	29.0	9.5	7.0	—	0.6	—	60	34	155	205	188	—	0.21	0.21	0.06	0.13	0.13	0.03	0.01	0.01	0.03	39
11081729	1990.0	—	2391.0	1802.4	90.7	5.9	6630	6534	6637	—	6661	6738	1.51	1.73	1.26	1.47	1.57	1.38	4.28	4.28	4.25	2,13,17
	84.0	24.9	18.5	—	1.4	—	60	55	207	84	166	—	0.31	0.31	0.03	0.11	0.11	0.02	0.01	0.01	0.03	39
11244118	1420.0	1526.8	1169.9	—	71.3	5.5	5745	5729	5491	5736	5868	—	1.33	1.32	1.10	1.69	1.69	1.59	4.10	4.10	4.09	2,13,17
	31.0	15.3	11.7	—	0.9	—	60	58	197	152	143	—	0.18	0.18	0.05	0.09	0.09	0.03	0.01	0.01	0.03	39

Table A1: – continued from previous page

Star	$\nu_{\rm max}$	$\nu_{\rm min0}$	$\nu_{\rm min1}$	$\nu_{\rm min2}$	$\langle\Delta\nu\rangle$	$\langle\delta\nu_{02}\rangle$	$T_{\rm eS}$	$T_{\rm eVK}$	$T_{\rm eBV}$	$T_{\rm sis0}$	$T_{\rm sis1}$	$T_{\rm sis2}$	$M_{\rm sca}$	$M'_{\rm sca}$	$M_{\rm lit}$	$R_{\rm sca}$	$R'_{\rm sca}$	$R_{\rm lit}$	$\log g_{\rm sca}$	$\log g'_{\rm sca}$	$\log g_{\rm spc}$	Ref
	μHz	μHz	μHz	μHz	μHz	μHz	K	K	K	K	K	K	$M_\odot$	$M_\odot$	$M_\odot$	$R_\odot$	$R_\odot$	$R_\odot$				
11253226	1638.0	2150.4	1684.6	1194.6	76.9	4.4	6410	6572	6768	6402	6520	6451	1.63	1.77	1.41	1.70	1.77	1.55	4.19	4.19	3.96	2,17,39
	48.0	21.5	16.8	11.9	1.0	—	125	38	156	41	68	118	0.28	0.28	0.05	0.11	0.11	0.02	0.01	0.01	0.21	40
11295426	2154.0	2233.4	1766.4	—	101.2	5.8	5793	5838	5712	5539	5773	—	1.16	1.15	1.08	1.28	1.28	1.24	4.29	4.29	4.28	27,29,46
	13.0	22.3	17.7	—	1.0	—	74	87	235	99	78	—	0.09	0.09	0.05	0.04	0.04	0.02	0.01	0.01	0.06	
11395018	834.0	875.3	685.2	—	47.3	4.2	5445	5517	5458	5566	5965	—	1.29	1.28	1.27	2.20	2.19	2.18	3.86	3.86	3.84	2,18,23
	50.0	8.8	6.9	—	0.5	—	85	101	376	345	264	—	0.31	0.31	0.04	0.19	0.19	0.02	0.01	0.01	0.12	
11414712	707.0	781.2	586.9	—	43.9	4.1	5635	5581	5563	5783	6063	—	1.11	1.10	1.26	2.20	2.20	2.34	3.80	3.80	3.80	2,13,17
	20.0	7.8	5.9	—	0.7	—	60	33	81	141	117	—	0.18	0.18	0.08	0.14	0.14	0.06	0.02	0.02	0.03	
11713510	1241.0	—	—	—	68.9	—	5893	5893	6055	—	—	—	1.05	1.05	1.00	1.60	1.60	1.57	4.05	4.05	—	17,37
	33.0	—	—	—	0.9	—	9	133	—	—	—	—	0.14	0.14	0.01	0.09	0.09	0.01	0.01	0.01	—	
11717120	585.0	583.7	434.3	—	37.8	4.2	5150	5034	5165	5263	5722	—	0.99	1.00	1.01	2.33	2.35	2.38	3.70	3.70	3.68	2,13,17
	8.0	5.8	4.3	—	0.9	—	60	42	140	128	87	—	0.15	0.15	0.10	0.16	0.16	0.11	0.02	0.02	0.03	
11771760	535.0	652.7	477.2	—	32.2	3.1	6142	—	—	6142	6246	—	1.81	1.87	1.55	3.16	3.22	3.00	3.70	3.70	—	2,17
	19.0	6.5	4.8	—	0.7	—	99	—	—	100	116	—	0.39	0.39	0.14	0.27	0.27	0.01	0.02	0.02	—	
11772920	3439.0	3709.5	—	—	157.4	8.7	5209	5371	5153	5790	—	—	0.68	0.68	—	0.80	0.80	—	4.47	4.47	4.34	2,40
	103.2	37.1	—	—	1.6	—	51	57	173	197	—	—	0.10	0.10	—	0.04	0.04	—	0.01	0.01	0.23	
11807274	1496.0	1678.7	1355.2	—	75.1	5.7	6225	6107	6365	5943	6232	—	1.35	1.42	1.26	1.63	1.67	1.58	4.14	4.14	4.13	16,29
	56.0	16.8	13.6	—	0.8	—	66	97	478	176	149	—	0.23	0.23	0.07	0.10	0.10	0.03	0.01	0.01	0.01	
12009504	1768.0	2003.2	1558.7	—	88.1	6.0	6099	6232	6022	5988	6139	—	1.16	1.20	1.12	1.40	1.42	1.38	4.21	4.21	4.00	2,17,39
	40.0	20.0	15.6	—	1.2	—	125	61	168	115	115	—	0.18	0.18	0.02	0.08	0.08	0.04	0.01	0.01	0.21	40
12069424	2101.0	2317.2	1802.2	—	103.4	5.8	5813	5790	5741	5874	6027	—	0.99	0.99	1.11	1.20	1.20	1.24	4.28	4.28	4.28	35,38,45
	63.0	23.2	18.0	—	1.0	—	18	—	—	166	162	—	0.13	0.13	0.02	0.06	0.06	0.01	0.01	0.01	0.02	
12069449	2552.0	2626.2	2114.5	—	116.7	6.6	5749	5745	5671	5493	5798	—	1.08	1.07	1.07	1.14	1.13	1.13	4.36	4.36	4.33	35,38,45
	76.6	26.3	21.1	—	1.2	—	17	—	—	260	212	—	0.14	0.14	0.02	0.06	0.06	0.01	0.01	0.01	0.02	
12258514	1440.0	1667.1	1251.8	—	74.5	4.9	5990	6017	6062	6052	6108	—	1.21	1.23	1.20	1.59	1.60	1.59	4.12	4.12	4.11	2,13,17
	43.0	16.7	12.5	—	0.8	—	60	—	—	121	141	—	0.18	0.18	0.08	0.09	0.09	0.04	0.01	0.01	0.03	39
12317678	1238.0	1681.9	1349.5	945.8	63.3	3.5	6401	6401	6760	6418	6588	6583	1.53	1.66	1.41	1.89	1.97	1.85	4.07	4.07	—	2,17
	40.0	16.8	13.5	9.5	0.8	—	99	39	153	36	48	87	0.26	0.26	0.13	0.12	0.12	0.06	0.01	0.01	—	
12508433	793.0	786.7	650.6	—	44.9	3.8	5134	5161	5062	5223	5959	—	1.22	1.24	1.17	2.23	2.25	2.20	3.83	3.83	3.50	2,17,40
	26.0	7.9	6.5	—	0.7	—	121	84	174	271	160	—	0.24	0.24	0.12	0.17	0.17	0.09	0.01	0.01	0.28	
2151	1000.0	1108.0	831.9	—	57.6	5.1	5790	5955	5762	5826	6021	—	1.10	1.10	1.08	1.83	1.83	1.81	3.95	3.95	3.84	8,11,12
	30.0	11.1	8.3	—	0.6	—	40	—	—	151	138	—	0.15	0.15	0.03	0.10	0.10	0.02	0.01	0.01	0.08	
43587	2247.0	2485.3	1965.2	—	106.4	6.0	5947	5835	5897	5905	6082	—	1.10	1.12	1.04	1.21	1.22	1.19	4.31	4.31	4.37	10,41
	15.0	24.9	19.7	—	1.1	—	17	79	64	71	63	—	0.07	0.07	0.01	0.03	0.03	0.04	0.01	0.01	0.04	
49385	1013.0	1154.8	881.3	—	56.3	4.1	6095	—	6241	5960	6146	—	1.31	1.35	1.25	1.96	1.99	1.94	3.97	3.97	4.00	19,20
	3.0	11.5	8.8	—	0.6	—	65	—	—	45	38	—	0.09	0.09	0.05	0.06	0.06	0.03	0.01	0.01	0.06	
49933	1760.0	—	2053.9	1670.8	86.1	2.2	6522	—	6922	—	6643	6768	1.29	1.43	1.28	1.45	1.53	1.46	4.23	4.23	4.00	1,34,47
	52.8	—	20.5	16.7	0.9	—	38	—	—	—	27	29	0.18	0.18	0.01	0.08	0.08	0.01	0.01	0.01	0.06	
52265	2090.0	2389.8	1808.0	—	98.1	8.2	6116	6096	6208	6054	6031	—	1.25	1.29	1.24	1.33	1.35	1.33	4.29	4.29	4.32	5,24,31
	20.0	23.9	18.1	—	1.0	—	110	—	—	67	80	—	0.12	0.12	0.02	0.05	0.05	0.02	0.01	0.01	0.20	
146233	3100.0	3202.1	2668.7	—	133.4	10.5	5693	6146	5680	5533	5943	—	1.12	1.11	1.03	1.05	1.05	1.02	4.44	4.44	4.48	7,32,47
	93.0	32.0	26.7	—	1.3	—	108	—	—	267	201	—	0.18	0.18	0.01	0.06	0.06	0.01	0.01	0.01	0.06	
181420	1610.0	—	1674.1	—	75.6	6.7	6580	6529	6590	—	6537	—	1.65	1.87	1.30	1.71	1.82	1.61	4.19	4.19	4.09	6,28,44
	10.0	—	16.7	—	0.8	—	100	53	109	—	26	—	0.13	0.13	0.17	0.06	0.06	0.10	0.01	0.01	0.15	
181907	28.5	24.2	—	—	3.5	0.7	4725	4744	4758	4741	—	—	1.30	1.41	1.43	12.42	12.91	12.93	2.37	2.36	2.35	15,26,30
	0.7	0.2	—	—	0.1	—	65	—	—	132	—	—	0.20	0.20	0.23	0.76	0.76	0.44	0.01	0.01	0.04	

Table A1: – continued from previous page

Star	$\nu_{\rm max}$	$\nu_{\rm min0}$	$\nu_{\rm min1}$	$\nu_{\rm min2}$	$\langle\Delta\nu\rangle$	$\langle\delta\nu_{02}\rangle$	$T_{\rm eS}$	$T_{\rm eVK}$	$T_{\rm eBV}$	$T_{\rm sis0}$	$T_{\rm sis1}$	$T_{\rm sis2}$	$M_{\rm sca}$	$M'_{\rm sca}$	$M_{\rm lit}$	$R_{\rm sca}$	$R'_{\rm sca}$	$R_{\rm lit}$	$\log g_{\rm sca}$	$\log g'_{\rm sca}$	$\log g_{\rm spc}$	Ref
	μHz	μHz	μHz	μHz	μHz	μHz	K	K	K	K	K	K	$M_\odot$	$M_\odot$	$M_\odot$	$R_\odot$	$R_\odot$	$R_\odot$				
203608	2600.0	—	2488.0	—	120.3	6.7	6253	6165	6266	—	6371	—	1.08	1.14	0.93	1.10	1.13	1.06	4.39	4.39	4.36	42,43
	0.5	—	24.9	—	1.2	—	32	—	—	—	26	—	0.05	0.05	0.01	0.03	0.03	0.01	0.01	0.01	0.01	
Procyon A	1014.0	—	1129.7	739.4	55.2	2.5	6530	6544	6633	—	6602	6546	1.46	1.63	1.48	2.03	2.15	2.03	3.99	3.99	4.05	48,49,50
	11.0	—	11.3	7.4	0.5	—	90	—	—	—	20	41	0.13	0.13	0.01	0.07	0.07	0.01	0.01	0.01	0.04	51,52,53
$\odot$	3050.0	3256.6	2555.2	1879.5	136.0	9.8	5777	—	—	5742	5831	5840	1.00	1.00	1.00	1.00	1.00	1.00	4.44	4.44	4.44	
	49.9	32.6	25.6	18.8	0.1	—	20	—	—	141	137	148	0.06	0.06	0.01	0.02	0.02	0.01	0.01	0.01	0.01	

Ref. – 1: Appourchaux et al.(2008), 2: Appourchaux et al.(2012), 3: Appourchaux et al.(2014), 4: Ballard et al.(2014), 5: Ballot et al.(2011), 6: Barban et al.(2009), 7: Bazot et al.(2012), 8: Bedding et al.(2007), 9: Benomar et al.(2014), 10: Boumier et al.(2014), 11: Brandão et al.(2011), 12: Bruntt et al.(2010), 13: Bruntt et al.(2012), 14: Campante et al.(2011), 15: Carrier et al.(2010), 16: Chaplin et al.(2013), 17: Chaplin et al.(2014), 18: Creevey et al.(2012), 19: Deheuvels et al.(2010), 20: Deheuvels & Michel(2011), 21: Deheuvels et al.(2012), 22: Deheuvels et al.(2014), 23: Doğan et al.(2013), 24: Escobar et al.(2012), 25: García et al.(2014), 26: Ghezzi & Johnson(2015), 27: Gilliland et al.(2013), 28: Hekker & Ball(2014), 29: Huber et al.(2013), 30: Lagarde et al.(2015), 31: Lebreton & Goupil(2014), 32: Li et al.(2012), 33: Lillo-Box et al.(2014), 34: Liu et al.(2014), 35: Lund et al.(2014), 36: Marcy et al.(2014), 37: Mathur et al.(2012), 38: Metcalfe et al.(2012), 39: Metcalfe et al.(2014), 40: Molenda-Żakowicz et al.(2013), 41: Morel et al.(2013), 42: Mortier et al.(2014), 43: Mosser et al.(2008), 44: Ozel et al.(2013), 45: Ramírez et al.(2011), 46: Santos et al.(2013), 47: Soubiran et al.(2010), 48: Aufdenberg, Ludwig & Kervella (2005), 49: Bond et al. (2015), 50: Huber et al. (2011a), 51: Bedding et. al. (2010), 52: Eggenberger et al. (2004), 53: Fuhrmann et al. (1997)